Efficient and Cost-effective Rating of Critical Members of Steel Truss Railroad Bridges Supported by Field Test Data

Final Report
October 2025

Principal Investigator: Ramesh B. Malla, Ph.D., F. ASCE, F. EMI, A.F. AIAA, M. CASE, Professor
School of Civil and Environmental Engineering
University of Connecticut

Authors
Rahul Anand (Graduate Assistant), Sachin Tripathi (Graduate Assistant), and
Ramesh B. Malla, Ph.D., F. ASCE, F. EMI, A.F. AIAA, M. CASE (Professor),
School of Civil and Environmental Engineering
University of Connecticut

Sponsored By
Transportation Infrastructure Durability Center
U.S. Department of Transportation, University Transportation Center Programs

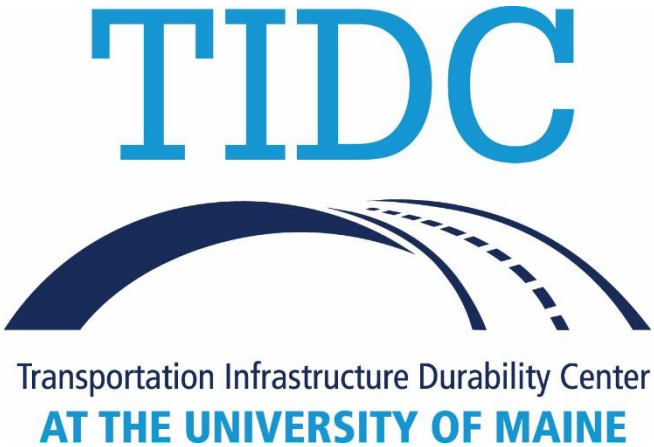

A Report From:
University of Connecticut
School of Civil and Environmental Engineering
261 Glenbrook Rd, Unit 3037,
Storrs, CT 06269-3037
Phone: (860) 486-2992
Website: https://cee.engr.uconn.edu

About the Transportation Infrastructure Durability Center

The Transportation Infrastructure Durability Center (TIDC) is the 2018 US DOT Region 1 (New England) University Transportation Center (UTC) located at the University of Maine Advanced Structures and Composites Center. TIDC's research focuses on efforts to improve the durability and extend the life of transportation infrastructure in New England and beyond through an integrated collaboration of universities, state DOTs, and industry. The TIDC is comprised of six New England universities, the University of Maine (lead), the University of Connecticut, the University of Massachusetts Lowell, the University of Rhode Island, the University of Vermont, and Western New England University.

U.S. Department of Transportation (US DOT) Disclaimer

Acknowledgements

Funding for this research is provided by the Transportation Infrastructure Durability Center at the University of Maine under grant 69A3551847101 from the U.S. Department of Transportation's University Transportation Centers Program. The principal investigator of the project would like to acknowledge and thank the following individuals and organizations whose support (financial, material, and/or in-kind) assisted in this research and significantly contributed to the success of the project:

University of Connecticut Graduate Assistants involved in this project:
Rahul Anand, School of Civil and Environmental Engineering
Sachin Tripathi, School of Civil and Environmental Engineering
Celso de Oliveira, School of Civil and Environmental Engineering

The following members of the project's Expert Panel for their time and attention by serving as technical champions and providing many valuable comments during the course of this project:

Mr. Haresh Dholakia, P.E., Transportation Engineering Supervisor, Rail Design (ConnDOT)
Mr. Manesh Dodia, P.E., Supervising Rail Officer, Rail Construction (ConnDOT)
Mr. Warren Best, P.E., Deputy Director- Structures (Metro-North Railroad Company), Retired
Mr. Randolph Pareja, P.E. Assistant Deputy Director- Structures (Metro-North Railroad Company)
Ms. Hong McConnell, P.E., Deputy Assistant Director – M.o.W – Structures/Capital (Metro-North Railroad Company)
Mr. Mario Pineda, Territory Manager (Polytec Inc.)

Mr. Rene Asuncion, P.E., Director Engineering-Structures Maintenance & Inspection (Amtrak)

The Connecticut Department of Transportation, Newington, CT for their in-kind support and providing technical input and feedback (Contact: Mr. Haresh Dholakia, P.E, Transportation Supervising Engineer, Rail Bridge Design, and Mr. Manesh Dodia, P.E., Supervising Rail Officer, Rail Construction).

Metro-North Railroad Company, Bridgeport, CT for in-kind support and providing technical input and feedback (Contact: Mr. Warren Best, P.E., Assistant Deputy Director - Structures (Retired), Mr. Randolph Pareja, P.E., Assistant deputy Director - Structures and Ms. McConnel Hong, P.E., Deputy Assistant Director – M.o.W – Structures/Capital).

Polytec, Inc., Hudson, MA, for providing in-kind support as well as technical input and feedback (Contact: Mario Pineda, Territory Manager).

Amtrak, Philadelphia, PA, for providing in-kind support, train specifications, and technical feedback. (Contact: René S. Asuncion, Sr. Principal Engineer - Structures Maintenance and Inspection).

Genesee & Wyoming Railroad, Northeast Region, Indianapolis, IN for supporting the project with technical input and feedback. (Contact: Chad R. Boutet, P.E, MBA, Director of Engineering – Grants).

New Hampshire Department of Transportation, Concordia, NH for supporting the project with technical input and feedback. (Contact: Chuck Corliss, P.E., Railroad Operations Engineer).

Special thanks to Sushrut Vaidya, Ph.D., Postdoctoral Research Associate (School of Civil and Environmental Engineering, University of Connecticut), for proofreading the report, providing valuable comments/edits, and revising the report to prepare the final version.

Last, but not least, the University of Connecticut, its Department of Civil and Environmental Engineering, and Connecticut Transportation Institute (CTI) for cost share, in-kind support, laboratory facilities, and project administration help.

Technical Report Documentation Page

1. Report No.	2. Government Accession No.	3. Recipient Catalog No.
4 Title and Subtitle Efficient and Cost-effective Rating of Critical Members of Steel Truss Railroad Bridges Supported by Field Test Data		**5 Report Date** October 31, 2025 **6 Performing Organization Code**
7. Author(s) Rahul Anand: https://orcid.org/0009-0007-4459-3345 Sachin Tripathi: https://orcid.org/0000-0002-3629-9679 Ramesh B. Malla: https://orcid.org/0000-0002-8035-8402		**8 Performing Organization Report No.**
9 Performing Organization Name and Address University of Connecticut, School of Civil & Environmental Engineering, 261 Glenbrook Road, Storrs, Connecticut 06269-3037, U.S.A.		**10 Work Unit No. (TRAIS)** **11 Contract or Grant No.**
12 Sponsoring Agency Name and Address U.S. DOT Region 1 University Transportation Center (UTC) -Transportation Infrastructure Durability Center (TIDC), ASCC, University of Maine, 35 Flagstaff Rd., Orono, Maine, U.S.A.		**13 Type of Report and Period Covered** Final report, October 01, 2023-September 30, 2025 **14 Sponsoring Agency Code**
15 Supplementary Notes		

16 Abstract

Assessing the load-carrying capacity of aging steel truss railroad bridges is challenging, due to significant uncertainties in material properties, deterioration, and support conditions. This study presents a comprehensive methodology for efficient, cost-effective load rating of critical bridge members through high-fidelity computational modeling, using the century-old Cos Cob Bridge in Connecticut as a case study. The approach integrates non-contact field measurements using Laser Doppler Vibrometer (LDV) with advanced finite element (FE) model updating. An initial FE model, developed from original design drawings, was calibrated using dynamic data (deflection time-histories and natural frequencies) collected under operational train loads. A sensitivity analysis first identified critical uncertain parameters, such as steel stiffness, joint flexibility, and support stiffness. These influential parameters were then systematically optimized using a real-coded genetic algorithm (RCGA) to minimize discrepancies between simulated and observed responses.

The resulting calibrated model accurately replicated the bridge's dynamic characteristics—including natural frequencies, mode shapes, and mid-span deflections—matching the LDV field data within a few percent. A refined load rating, performed on the validated model in accordance with AREMA standards, confirmed that the bridge meets current operational safety requirements. This research demonstrates that combining advanced non-contact diagnostics with sensitivity-guided optimization provides a robust framework for accurate load capacity assessment, ultimately supporting more reliable infrastructure management decisions.

17 Key Words	18 Distribution Statement
Finite element (FE) modeling; Sensitivity analysis; Genetic algorithm; Model updating; Field testing; Laser Doppler Vibrometer (LDV);, Load rating;, Critical members	No restrictions.

19 Security Classification (of this report)	20 Security Classification (of this page)	21 No. of pages	22 Price
Unclassified	Unclassified	52	

Form DOT F 1700.7 (8-72)

Table of Contents

List of Figures

List of Tables

List of Key Terms

Finite element (FE) modeling; Sensitivity analysis; Genetic algorithm; Model updating; Field testing; Laser Doppler Vibrometer (LDV).

Abstract

Assessing the load-carrying capacity of aging steel truss railroad bridges is challenging due to significant uncertainties in material properties, deterioration, and support conditions. This study presents a comprehensive methodology for the high-fidelity modeling of these structures, using the century-old Cos Cob Bridge in Connecticut as a case study.

The approach integrates non-contact field measurements using Laser Doppler Vibrometry (LDV) with advanced finite element (FE) model updating. An initial FE model, developed from original design drawings, was calibrated using field test data (vertical deflection and natural frequency) collected under operational train loads. A sensitivity analysis first identified critical uncertain parameters, such as steel stiffness, joint flexibility, and support stiffness. These influential parameters were then systematically optimized using a real-coded genetic algorithm (RCGA) to minimize discrepancies between simulated and observed responses.

The resulting calibrated model accurately replicated the bridge's dynamic characteristics—including natural frequencies, mode shapes, and mid-span deflections—matching the LDV field data within a few percent. A refined load rating, performed on the validated model in accordance with AREMA standards, confirmed the bridge meets current operational safety requirements. This research demonstrates that combining advanced non-contact diagnostics with sensitivity-guided optimization provides a robust framework for accurate load capacity assessment, ultimately supporting more reliable infrastructure management decisions.

Chapter 1: Introduction and Background

1.1 Project Motivation

Aging railway bridges in the United States pose a critical challenge to transportation infrastructure. Many steel truss railroad bridges, built in the late 19th and early 20th centuries, are still in service, well beyond their intended design lives. As of 2020, approximately 7.6% of the nation's 616,087 bridges were classified as structurally deficient, indicating key elements in poor condition [1]. This issue is exacerbated by steadily increasing traffic demands, heavier axle loads, and higher train speeds that impose stresses far beyond what the original designers envisioned. The combination of advanced age and modern operational demands raises pressing safety and serviceability concerns. When deterioration is not properly assessed and managed, the consequences can range from costly service disruptions to catastrophic failures. Historical failures such as the sudden collapse of the Silver Bridge in 1967 [2] and the I-35W Mississippi River Bridge in 2007 [3] underscore the tragic potential of undetected deficiencies in aging steel bridges. These events highlight an urgent mandate for more reliable assessment of legacy bridge structures to prevent loss of service and life.

Steel truss bridges like the Cos Cob Bridge in Greenwich, CT—an over-century-old railroad bridge on the Northeast Corridor—embody the challenges of aging infrastructure. Decades of service under harsh environmental exposure and millions of loading cycles have introduced significant uncertainties in its structural properties and behavior. Critical material characteristics are often unknown or variable; for example, the Cos Cob Bridge's original construction steel (specified as ASTM A7 from early 20th-century practice) may have a present-day elastic modulus and strength that differ markedly from nominal values due to material aging. Moreover, such historic bridges endure progressive section loss from corrosion and accumulate fatigue damage under repetitive loadings [4]. Common issues documented in aging truss bridges include loosening or cracking of rivets, gusset plate deterioration, and reduced connection rigidity, all of which can alter load paths and dynamic properties of the structure [5]. These forms of degradation often remain hidden and are difficult to quantify through routine visual inspections alone, meaning that a bridge may exhibit unexpected behavior under trains, which is not evident from outward inspection [6]. In short, conventional inspection and analysis methods struggle to capture the true capacity and performance of a century-old truss bridge that has experienced myriad modifications, repairs, and deterioration over its life.

The presence of such uncertainties undermines the reliability of purely analytical models if they are not calibrated with real data. An uncalibrated finite element (FE) model based on idealized assumptions might yield predictions that are either overly conservative (leading to unwarranted load restrictions or expensive retrofits) or dangerously unconservative (failing to predict critical vulnerabilities in the structure). Bridge owners and engineers are therefore motivated to seek robust assessment techniques that can narrow this gap between theoretical predictions and actual structural behavior. In recent years, structural health monitoring (SHM) has emerged as a powerful approach to track bridge performance in real time, using sensor data to inform maintenance decisions and avert unnecessary load restrictions [7]. The cutting-edge concept of a digital twin – a living computational model updated continuously with sensor inputs – has further demonstrated the potential for proactive management of complex bridge systems [8,9]. However, implementing

continuous monitoring or full digital twin systems on every aging bridge may be impractical due to cost and logistical constraints. This reality underscores the significance of targeted field testing and model-updating strategies as practical and effective tools for infrastructure assessment. By integrating empirical field data with analytical modeling, engineers can transform an idealized computational (FE) model into an evidence-based representation of the bridge's current (i.e., actual) condition. In the case of the Cos Cob Bridge, this data-driven model serves as a virtual replica of the structure in its as-is state, providing a reliable basis for critical engineering evaluations such as load rating, life-safety analysis, and retrofit planning. The urgency to ensure safe operation of this vital rail link, while avoiding either undue conservatism or unsafe assumptions, forms the core motivation for the present research.

1.2 Research Objectives and Tasks

Drawing on the above motivation, the main objective of this research is to develop and demonstrate a rigorous framework for field-test-informed finite element (FE) model updating, and capacity evaluation (load rating) of critical members of an aging steel truss railroad bridge using the updated FE model. In particular, the study uses the Cos Cob Bridge as a case example to show how targeted experimental data can significantly improve the fidelity of analytical-computational models and thereby yield more accurate assessments/predictions of structural performance. The successful attainment of these objectives should contribute to enhancement of the safety assessment of the Cos Cob Bridge, as well as illustrate a methodology that can be generalized to similar aging infrastructure. Specifically, attainment of the aforementioned objectives involves the following steps:

1. Development of a high-fidelity finite element model of the Cos Cob steel truss railroad bridge and validation of the model through calibration with field test data, so that the model accurately reproduces the bridge's true global response under service loading. This entails adjusting the model to reflect the actual stiffness, mass, and boundary/support conditions of the in-situ structure, ensuring that key response parameters (e.g., deflected shapes, natural frequencies) match measured values within acceptable tolerances.

2. Utilizing the calibrated model to perform a comprehensive load rating analysis in accordance with the American Railway Engineering and Maintenance-of-Way Association (AREMA) guidelines. This analysis should contribute to determination of the bridge's safe load-carrying capacity for both standard design train loading scenarios and the specific modern train configurations (e.g., Metro-North commuter trains and Amtrak intercity trains) it currently carries, providing a well-substantiated basis for operational decision-making.

Research tasks:

To achieve these objectives, the research is structured into several interrelated tasks, combining experimental field work with analytical-computational modeling and optimization:

1. Finite Element Modeling: Development of a detailed three-dimensional FE model of the bridge, based on original design drawings and any available as-built information. This

initial model serves as the starting point for analysis, acknowledging that it may not yet capture the true in-service behavior of the aged structure.

2. Model Updating: Utilization of field test data, collected during the completion of previous U.S. DOT UTC-TIDC research projects, to perform a sensitivity-based calibration of the FE model. In this step, key uncertain parameters—such as material elastic modulus, member stiffness, support constraints, and mass distribution—are systematically adjusted to minimize the discrepancy between the model's predicted responses and the measured field data. A real-coded genetic algorithm (RCGA) optimization is employed to iteratively search for the optimal set of parameters, guided by sensitivity analysis, until the simulated bridge response (e.g., vertical deflection profiles/time histories and modal frequencies) match the observed behavior closely. This updated model thus learns from the physical bridge, reducing epistemic uncertainty in the analysis.

3. Load Rating: Utilization of the calibrated FE model as a reliable proxy for the actual bridge to carry out a load rating evaluation following AREMA-recommended practices for railroad bridges. The updated model is subjected to various loading scenarios, including standard design loads (such as the Cooper E80 load model (Figure 1)) and representative service trains (Metro-North M8 commuter trains, Amtrak Regional and Acela trains). For each case, the internal member forces and stresses computed by the model are used to calculate rating factors, which indicate the bridge's capacity to safely carry those loads. The outcome of this task is a set of rating values (e.g. Normal and Maximum Rating per AREMA definitions) for critical bridge members, identifying any capacity deficiencies and verifying whether the bridge meets required safety margins under current and future traffic demands.

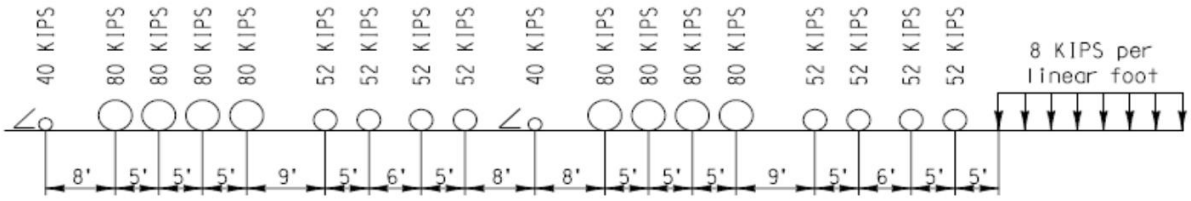

Figure 1: Cooper E 80 Loading, maximum axle load 80 kips (from AREMA 2014)

Through these integrated tasks, the research delivers both an enhanced understanding of the Cos Cob Bridge's structural behavior and a generalizable approach for bridging the gap between idealized models and real-world performance in aged bridge structures.

1.3 Report Overview

This report is organized as follows to reflect the progression from background context to methodology and findings of the research:

- Chapter 1 introduces the research problem and motivation, outlines the objectives and scope of the work, and provides an overview of the report structure (the present chapter).
- Chapter 2 describes the overall methodology adopted in this study. It defines the integrated approach for field testing and FE model development, and it details the strategy for sensitivity-based model updating. The chapter also outlines the experimental design, instrumentation plan for the Cos Cob Bridge field test, and the computational procedures used to update the model and evaluate load ratings.
- Chapter 3 details the field-testing campaign and the development of the initial finite element model. It documents the on-site testing of the Cos Cob Bridge, including the placement of instruments, data acquisition techniques, and the processing of the measured response data. The chapter then presents the development of the baseline FE model, discussing assumptions made and initial validation checks. A preliminary comparison between the model's predictions and the field measurements is included to highlight discrepancies before calibration.
- Chapter 4 focuses on the core process of model updating and the subsequent load rating analysis. This chapter explains the implementation of the sensitivity analysis and the real-coded genetic algorithm used to update the FE model parameters. It describes how the optimization was set up to match the bridge's measured deflection and vibration characteristics. Once the model updating results are obtained, Chapter 4 introduces the AREMA-based load rating procedure and details how the calibrated model is employed to compute the rating factors for the bridge. This section effectively links the improved analytical-computational model to practical capacity assessment outcomes.
- Chapter 5 presents the results and discusses the key findings of the research. It evaluates the performance of the updated FE model against independent portions of the field test data, demonstrating the degree of improvement in predictive accuracy. The chapter then reports the load rating results for the Cos Cob Bridge, identifying the governing load cases and critical members from the analysis. In addition, Chapter 5 provides a synthesis of what these results imply for the bridge's fitness for service and safety. Finally, the chapter (and the report) concludes with overarching conclusions, implications for bridge management, and recommendations for future work. By summarizing contributions and suggesting areas for further research (such as applying the framework to other bridges or integrating continuous monitoring), the report closes by emphasizing the broader significance of the study in advancing structural assessment practices.

Chapter 2: Methodology

2.1 Overview of the Integrated Research Framework

The research employs an integrated framework to assess the real structural behavior and the load-carrying capacity of a historic railroad bridge. The approach integrates field data collection with computational modeling and updating, ensuring that the final model simulates the real-world behavior of the structure to a high degree of accuracy.

The principal phases of the methodology are:

1. Finite Element Modeling and Initial Validation: Creating a baseline numerical model of the bridge based on design documents and identifying the initial discrepancies between its predictions and the field data obtained from the U.S. DOT UTC _TIDC Project# 1.13 [10].
2. Sensitivity Analysis and GA-Based Model Updating: Identifying the most influential uncertain parameters and using a global optimization algorithm to calibrate them, thereby creating a high-fidelity "digital twin" of the structure.
3. Load Rating Analysis using Updated Model: Utilizing the calibrated, validated, and updated model as a robust analytical tool to perform a comprehensive load rating in accordance with established industry standards.

This structured approach ensures that the final assessment is not merely based on idealized computational estimates, but on evidence-based evaluations that reflect the true, as-is condition of the aging infrastructure.

2.2 Finite Element Modeling

A detailed three-dimensional (3D) Finite Element (FE) model of the bridge superstructure was developed using the commercial software package ANSYS. The geometry and member cross-sections were based on the original 1904 as-built drawings. The initial model was constructed using a set of engineering assumptions for the parameters that were not precisely known. This included assigning nominal material properties for early 20th-century steel (ASTM A7) and idealizing the support boundary conditions as a combination of pinned and roller supports. The initial validation phase involved running dynamic and eigenvalue analyses on this baseline model, simulating the response of the bridge under the passage of a Metro-North M8 train as well as in free vibration. The resulting simulated deflections and natural frequencies were then compared directly to the values extracted from the field tests. This comparison quantified the initial discrepancies and confirmed that the baseline model was significantly stiffer than the actual structure, thereby establishing the necessity for the model updating procedure.

2.3 Sensitivity Analysis for Model Updating

Sensitivity analysis is a fundamental step in finite element model updating, enabling the identification of parameters that most significantly influence structural responses such as deflections and natural frequencies. By systematically perturbing uncertain parameters within realistic bounds and observing their effects on key outputs, the analysis prioritizes variables that

are both influential and identifiable. This focused approach improves computational efficiency and ensures a well-posed calibration process, particularly important in complex or aging structures where numerous uncertainties exist.

Mathematical Formulation

Let $\theta = [\theta_1, \theta_1, \dots \dots . \theta_n]$ represent the vector of model parameters to be updated (e.g., stiffness, mass, or boundary conditions). The finite element (FE) model predicts system responses $\mathrm{r_{model}}(\theta)$, and field monitoring provides corresponding measured responses $\mathrm{r_{exp}}$. The FE model updating task can be performed by minimizing a discrepancy function:

$$\Phi(\theta) = \| \mathrm{r_{exp}} - \mathrm{r_{model}}(\theta) \| \quad (3)$$

where $\|\cdot\|$ is typically a Euclidean or weighted norm [11,12]. Gradient-based methods approximate the partial derivatives of each model response r_i with respect to each parameter θ_j, which are the entries/elements of the sensitivity matrix S:

$$\mathrm{S_{ij}} = \frac{\partial \mathrm{r_i}}{\partial \theta_\mathrm{j}} \quad (4)$$

These derivatives form the sensitivity matrix, whose structure reveals how variations in parameters influence different outputs. Singular Value Decomposition (SVD) of this matrix can be used to identify rank deficiency or linear dependencies, helping to screen out poorly identifiable parameters [11].

Iterative Updating Procedure Using Real-Coded Genetic Algorithm (RCGA)

A hybrid approach combining direct sensitivity analysis with a genetic algorithm (GA) was used to update the FE model. Traditional gradient-based algorithms would update the parameter vector (θ) iteratively; for example, using a steepest-descent type update:

$$\theta^{(k+1)} = \theta^{(k)} - \alpha^{(k)}(S^T W)\nabla\Phi(\theta^{(k)}) \quad (5)$$

where $\alpha^{(k)}$ is a step size, W is a weighting matrix, and $\nabla\Phi$ is the gradient of the discrepancy function [12]. Alternatively, heuristic approaches (e.g., genetic algorithms) are employed for highly nonlinear parameter spaces [13].

In the RCGA implementation, the optimization began with an initial population of real-valued candidate solutions, each representing a possible set of values for the selected model parameters [e.g., Young's modulus (E), density (ρ), cross-sectional area (A), and support stiffness (k)]. To maintain physical realism while capturing parameter uncertainty, the initial population was generated by random sampling from log-normal distributions centered around nominal values. The log-normal formulation ensured positivity and allowed asymmetric variation, reflecting practical scenarios, such as material degradation or corrosion, which often reduce properties rather than increase them. The evolutionary process proceeded through the following steps:

1. Initial Population and Fitness Evaluation: Each candidate's parameter set was fed into the FE model, and the resulting global responses (vertical peak displacement at different locations) were compared with field measurements. A discrepancy function $\Phi(\theta)$ quantifying the mismatch between model and measured responses was used to evaluate fitness (with lower $\Phi(\theta)$ indicating a better fit).

2. Selection of Best Parameters: Using roulette wheel selection, individuals were probabilistically chosen for reproduction based on their fitness. This ensured that better-performing candidates had a higher chance of contributing to the next generation, while maintaining diversity in the gene pool.
3. Crossover and Mutation: Selected parent parameter sets underwent crossover (e.g., uniform crossover) to produce offspring (children) by combining genetic material from two parents. Additionally, mutation operations—small random perturbations based on the Gaussian distribution—were applied to explore the parameter space locally and avoid premature convergence.
4. Generation of Elite Offspring: The offspring (children) were then combined with the parent population and sorted based on their fitness function to preserve the original population sample size while generating quality offspring. This increases the convergence toward the optimized parameters.

This process was repeated for multiple generations until convergence criteria (ε) were met, either a negligible improvement in fitness between successive generations or the completion of a predefined number of iterations. The resulting optimized parameter set minimizes the discrepancy function $\Phi(\theta)$ and enables the updated FE model to more accurately replicate the measured global responses. A summary of the key RCGA parameters used in this study is provided in Table 1. The schematic flowchart of this procedure is provided in Figure 2.

Table 1: Real-Coded Genetic Algorithm (RCGA) Parameters Used in Sensitivity-Based Model Updating Procedure

Parameter	**Value**	**Justification**
Population size	12 sets per iteration	Balances exploration of parameter space and computational cost for FE analysis
Number of Generations	User-defined (until convergence or fitness plateaus)	Allows sufficient refinement of solutions while keeping runtime manageable
Crossover Rate	Arithmetic average (50–50 blend)	Simple, stable method to combine genetic material from two parents
Mutation Rate	5% (per parameter)	Maintains diversity and avoids local optima without disrupting convergence
Initial Distribution	Log-normal distribution	Reflects physical constraints (positivity) and realistic degradation behavior
Selection Method	Roulette Wheel	Ensures probabilistic bias toward better solutions while preserving diversity

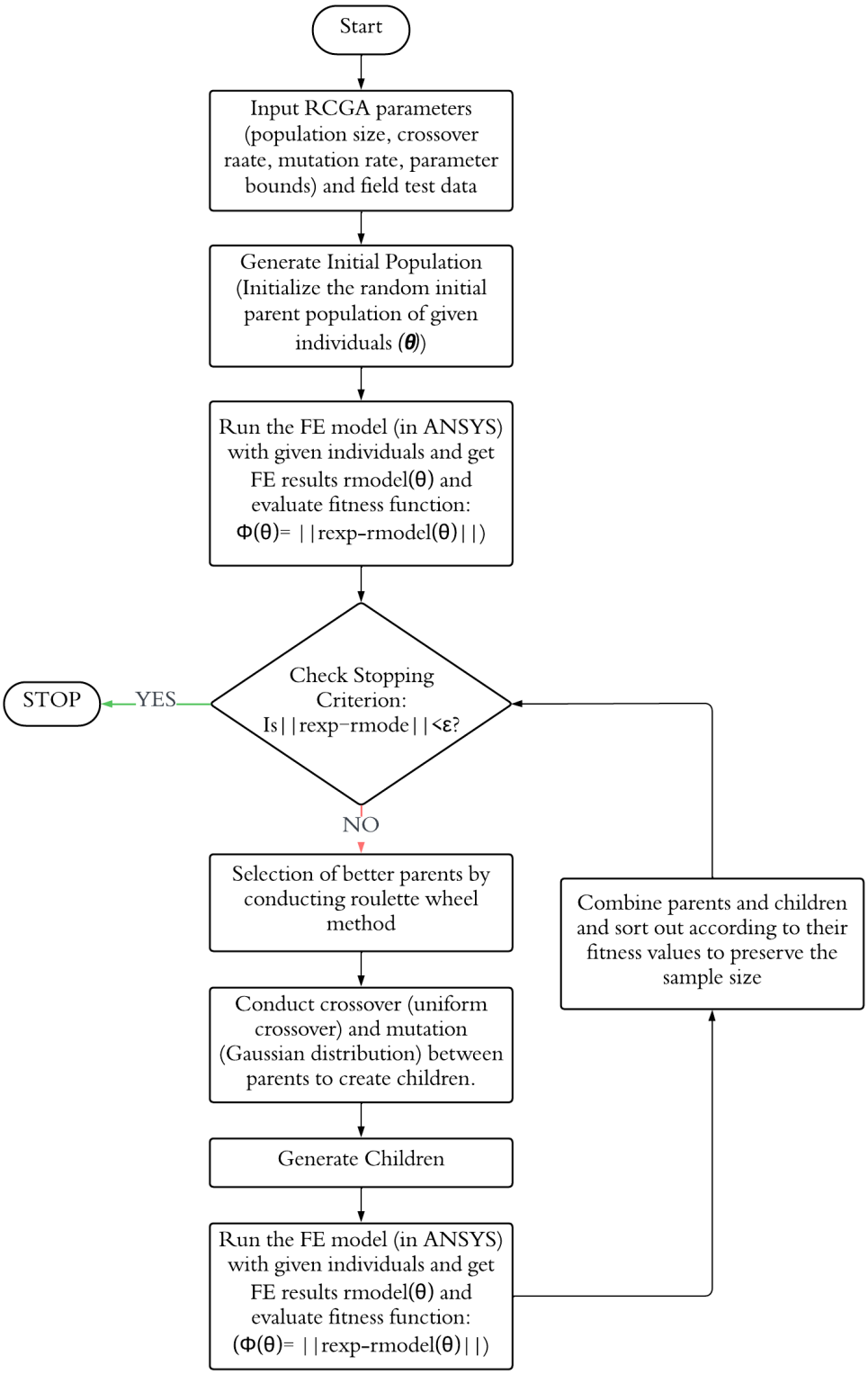

Figure 2: Real-Coded Genetic Algorithm (RCGA) Optimization Process for Updating the Finite Element Model of the Bridge Structure

Convergence and Validation

Model updating concludes when a convergence criterion is met, such as:

- Error Tolerance: The norm of the difference between experimental results and model predictions, $\|r_{exp} - r_{model}\|$, falls below a predefined threshold (indicating an acceptably small discrepancy). In this study, the threshold was set to 1% of the experimental value, which reflects an acceptable level of discrepancy based on typical measurement uncertainty and modeling assumptions used in similar structural calibration studies. This threshold was selected to ensure that the updated finite element model closely replicates the measured structural response without over-fitting.
- Parameter Stability: The changes in parameter values between successive GA generations becomes very small, suggesting the algorithm has converged on an optimal or near-optimal solution.
- Physical Reasonableness: The optimized parameters remain within realistic engineering limits. In practice, this meant that the GA results were checked to ensure, for example, that the adjusted Young's modulus was still within a few percent of the expected value for steel, or that the implied section loss or support stiffness was reasonable and could be explained by actual bridge conditions.

Once a converged set of parameters was obtained, the final step was to validate the updated model against independent data or metrics not explicitly used in the calibration. In this study, the validation was performed by comparing the updated model's predictions to field measurements for different train cases (trains that were not the basis of the optimization) and by checking additional response characteristics like frequencies. Close agreement in these comparisons increases confidence that the model updating improved the model in a general sense rather than over-fitting to a specific scenario.

2.4 Load Rating Analysis using Updated Model

In the final phase of the research, a load rating of the bridge was performed using the updated FE model. The load rating analysis followed the Allowable Stress Method as suggested by the AREMA manual, Chapter 15 [23]. The calibrated, updated 3D FE model was used to compute the internal forces in all the members. The standard Cooper E80 loading was used as a baseline, along with other passenger trains, including Metro-North M8, Amtrak Regional, and Amtrak Acela trains. A moving load analysis was performed to determine the maximum live load plus impact forces and stresses in each member. The stresses were compared to the allowable stresses for Normal and Maximum Rating per the AREMA manual for each member. For normal rating, allowable stresses are based on AREMA Chapter 15, Part 1-Design, Table 15-1-11, whereas, for maximum rating, allowable stresses are allowed to be increased as per AREMA Chapter 15, Table 15-7-1. Table 2 presents the allowable stresses for flexure and shear for normal and maximum ratings. The analysis provided a definitive and reliable assessment of the bridge's safe load-carrying capacity.

Table 2: Allowable Stresses for Normal and Maximum Rating

Stress type	**Allowable stress (normal rating)**	**Allowable stress (maximum rating)**
Flexural tension	$0.55f_y$	$0.8f_y$
Flexural compression	$0.55f_y - \frac{0.55{f_y}^2}{6.3\pi^2 E}\left(\frac{l}{r_y}\right)^2$ Or $\frac{0.131\pi E A_f}{ld(1+\mu)}$ Whichever is larger, but not to exceed $0.55f_y$	$0.8f_y - \frac{0.8f_y}{1.8\times 10^9}\left(\frac{l}{r_y}\right)^2$
Shear	$0.35f_y$	$0.75(0.8f_y)$

f_y - yield strength (psi)

E - modulus of elasticity (psi)

l - distance between points of lateral support for the compression flange (inch)

r_y - minimum radius of gyration of the compression flange and that portion of the web area on the compression side of the axis of bending, about an axis in the plane of the web (inch)

A_f - area of the smaller flange excluding any portion of the web (inch^2)

d – overall depth of the member (inch)

μ – Poisson's ratio

The formula to compute the rating factor is:

$$Rating\ Factor = \frac{Allowable\ Stress}{Live\ Load\ Stress} \quad (6)$$

Chapter 3: Field Testing, Initial Finite Element Modeling, and Results

3.1 Bridge Structure Investigated

This research focuses on a representative example of this ageing infrastructure class: the Cos Cob Bridge. The bridge is located on the Mianus River in Greenwich, Connecticut (Figure 2). This is a long-span, open-deck truss railroad bridge (Figure 3) and is a vital link in Amtrak's Northeast Corridor (NEC). The bridge was built in 1904 by the American Bridge Company, and it has been in continuous operation for over a century, carrying both commuter and high-speed intercity trains. The bridge is commonly used by passenger trains like Metro-North M8 (MTNR M8), Amtrak Regional, and Acela Express. The bridge has eleven simply supported spans resting on ten stone piers and two abutments at the ends. Three of the sections are deck girder, seven are deck trusses, and one is a rolling lift bascule. The bridge has four tracks (Track 1, Track 2, Track 3, and Track 4), and each track sits on a separate parallel bridge. The track system on the bridge consists of steel rails mounted on timber sleepers (cross-ties), which are supported on the bridge deck. The rails are secured to the sleepers using conventional rail fastening systems to maintain proper alignment and load transfer. As such, it embodies the challenges associated with historic railway bridges and serves as an ideal case study for the development and application of modern structural assessment methodologies.

This study focuses on Track 4 of span 3 (Figure 4) because of its accessibility for field testing equipment, especially during periods of lowered water levels affected by tides. Span 3 is 37.5 m (122’-10”) long. The height of the span is 4.57 m (15’), and the width is 2.3 m (7.5’). The bridge members’ cross-sections are typical I and C sections. The cross sections of the bridge members are presented in Appendix A.

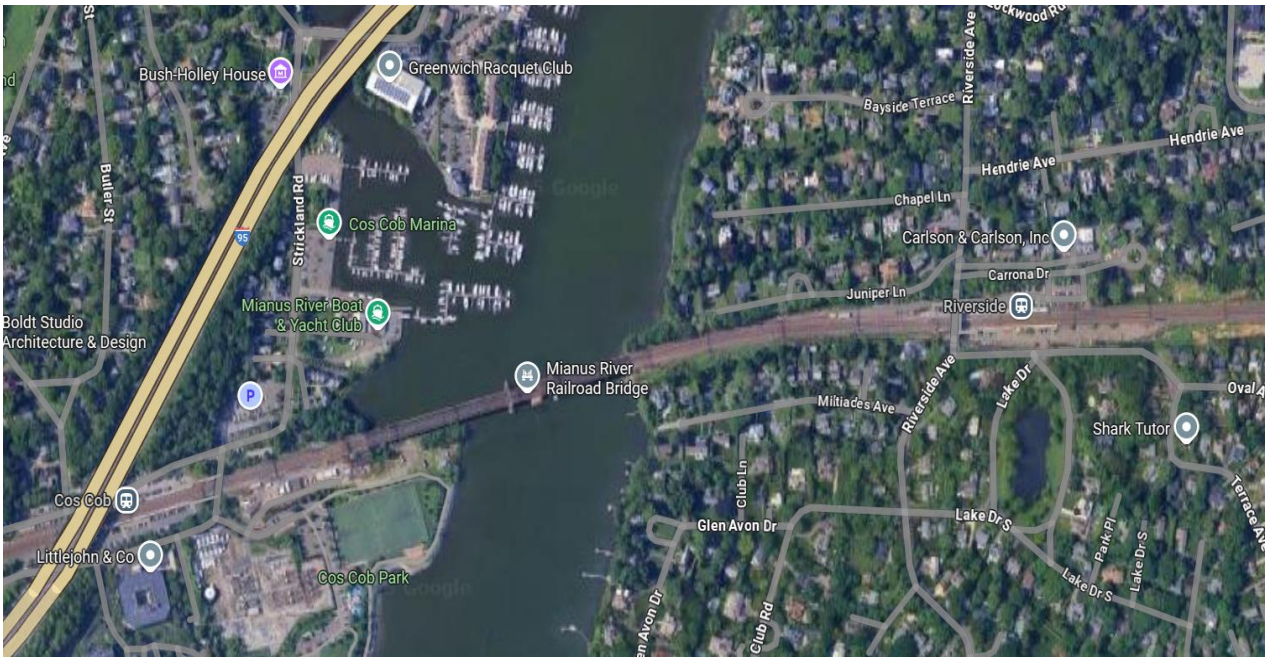

Figure 2: Location of the Cos Cob Bridge Across the Mianus River, Greenwich, CT (Source: Google Maps, http://maps.google.com)

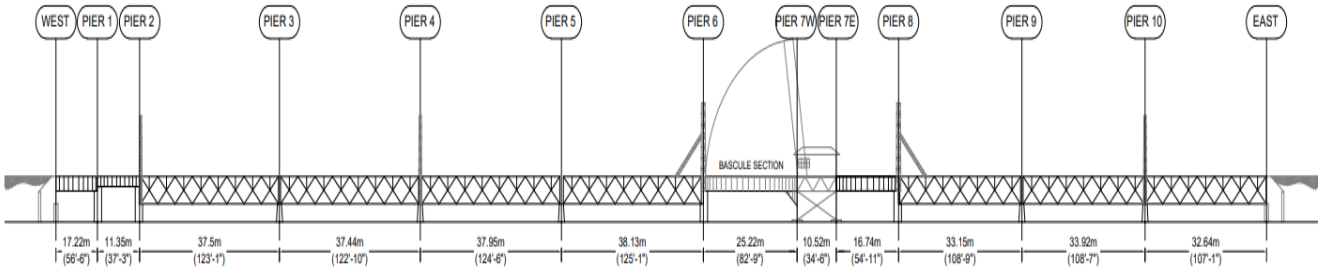

Figure 3: Cos Cob Bridge Elevation View *[14]*.

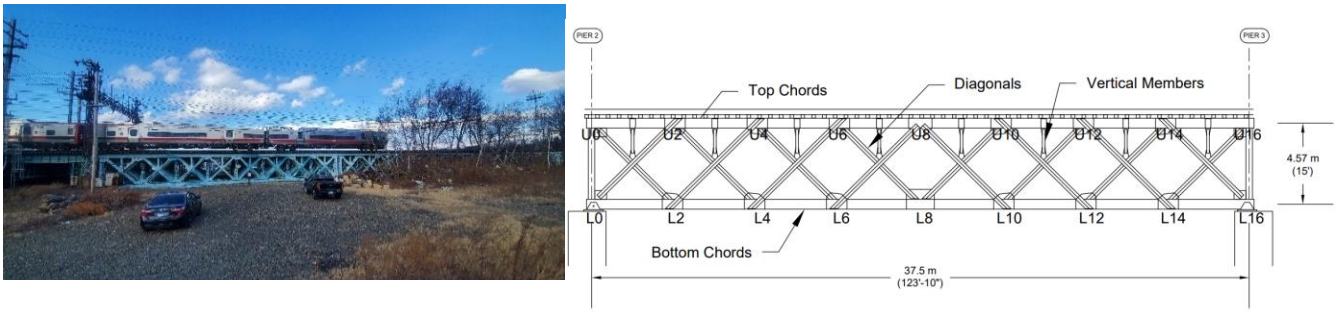

(a) (b)

Figure 4: Span 3 of Cos Cob Bridge: (a) Picture, (b) elevation view drawing *[14]*

3.2 Field Testing and Data Collection

Field testing and data collection were part of Project 1-13, and the test results required for this project were obtained for Project 1-13 [10]. Field tests were conducted during normal service with trains of three types: Metro-North M8 commuter train, Amtrak's Northeast Regional, and Amtrak's Acela Express. A single-point Laser Doppler Vibrometer (LDV) was used to perform field testing on the bridge. An LDV is a non-contact optical instrument that emits a laser beam to measure surface vibration by detecting the Doppler shift in the reflected beam. The single-point LDV was mounted on a tripod beneath the span, aiming upward at the underside of the Track 4 structure (Figure 5), to measure vertical velocity during train crossings. The LDV was repositioned between tests to collect data at multiple points along the span. Specifically, bridge responses (velocity) were recorded at three different locations on span 3 (Track 4), designated as Vib 1, Vib 2, and Vib 3 (Figure 6), where displacement results were desired. The LDV output was collected using a high-speed data acquisition system, with sampling conducted at 512 Hz to adequately capture both forced and free vibration signals during and after the passage of a train. Data were recorded in the time domain using a Polytec PSV® data acquisition system and then processed in MATLAB®. Multiple train traversals were recorded at each sensor position to ensure reliable data under consistent operating conditions. All tests were performed with trains traveling from New York toward New Haven (west-to-east direction).

Figure 5: Laser Doppler Vibrometer (LDV) setup to record vertical displacement of the bridge during train traversal.

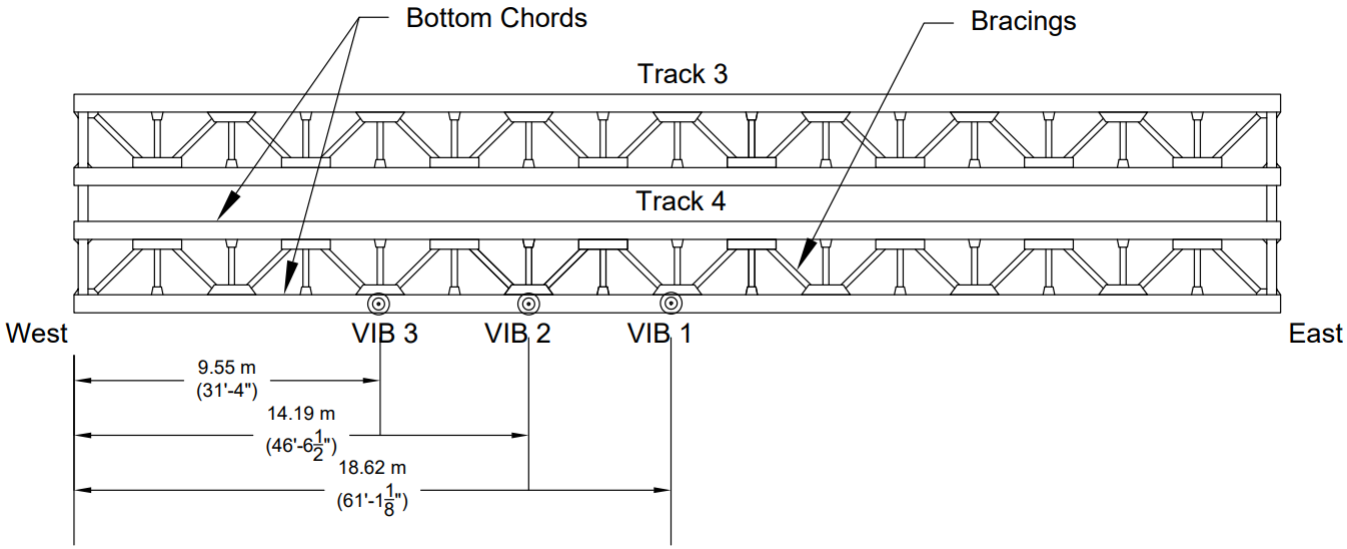

Figure 6: Cos Cob Bridge plan view (Track 4): Vib 1, Vib 2, and Vib 3 represent nodes where the responses were collected using LDV.

3.3 Development of the Finite Element Model

A detailed three-dimensional (3D) Finite Element (FE) model of Span 3, Track 4 of the Cos Cob Bridge was developed using the commercial FE analysis software ANSYS®. The model was created to serve as a computational platform for simulating the bridge's structural response, which could then be compared against the field-measured data. The development process involved careful consideration of the model's geometry, element types, material properties, and boundary conditions.

3.3.1 Geometry, Meshing, and Element Selection

The fundamental geometry of the FE model was derived from archival documents, including the original as-built drawings from 1904 and past load rating reports [15]. This ensured that the spatial arrangement and dimensions of the truss members accurately reflected the design intent. Figure 7(a) shows the idealized 3D wireframe model of the truss, and Figure 7 (b) shows a rendered view of the model. The cross-sections assigned to the members are presented in Appendix A.
The selection of appropriate element types is crucial for capturing the correct structural behavior. For this model, a mixed-element approach was used:

- *BEAM188 Elements:* The primary load-carrying members of the truss, including the top and bottom chords, verticals, and diagonals, were modeled using beam elements. These elements are formulated based on Timoshenko beam theory and possess six degrees of freedom at each node (three translations and three rotations), allowing them to accurately represent axial, shear, and bending behavior.

- *LINK180 Elements:* The secondary bracing members, which are designed to carry only axial loads (tension or compression), were modeled using truss elements. These elements have only translational degrees of freedom and provide a computationally efficient way to represent axially loaded members.

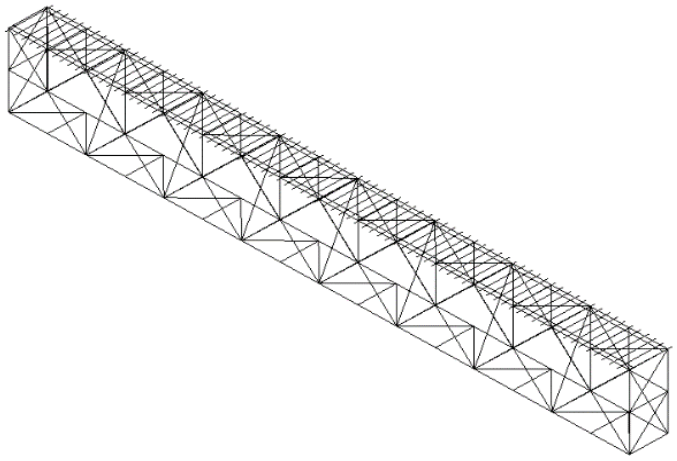

(a)

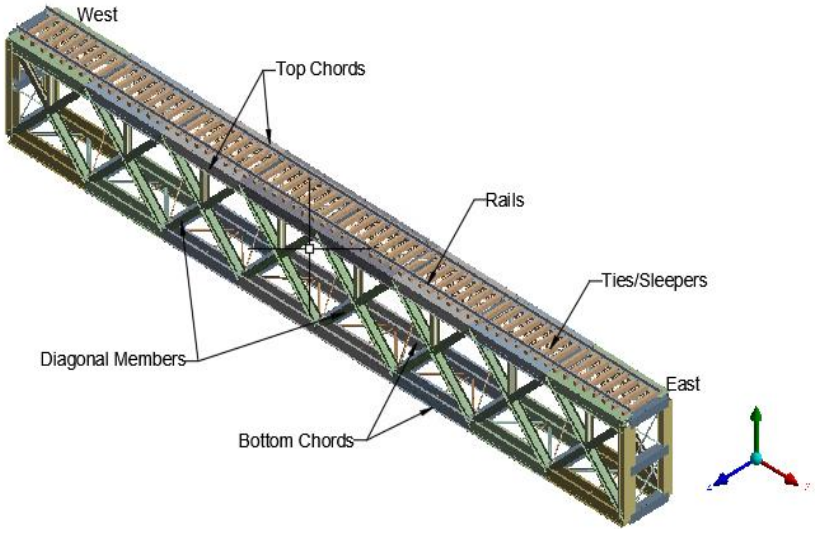

(b)

Figure 7: Cos Cob Bridge FE Model: (a) 3D Wire Model; (b) Rendered View

3.3.2 Material Properties

A significant source of uncertainty in modeling historic structures is the definition of material properties. The primary structural material for the Cos Cob Bridge is structural steel meeting the ASTM A7 specification, which was common for early 20th-century construction. For the initial, uncalibrated model, nominal material properties for this type of steel were assigned. However, the actual in-situ properties, after more than a century of service, are unknown and are treated as key parameters to be refined during the model updating process. The model also included timber sleepers (railroad ties), which were assigned the properties of oak wood. The nominal properties assigned to all materials in the initial model are summarized in Table 3.

Table 3: Bridge Material Properties used in the FE model.

Material Structural Parameters	**Structural Steel**	**Oak Wood**
Young's Modulus (N/m^2)	2×10^{11}	2.278×10^{10}
Poisson's Ratio	0.3	0.3742
Tensile Ultimate Strength (N/m^2)	4.6×10^{8}	1.467×10^{8}
Tensile Yield Strength (N/m^2)	2.5×10^{8}	4.776×10^{7}
Density (kg/m^3)	7850	935.7

3.3.3 Boundary Conditions and Connections

The representation of supports and connections is critical to accurately simulating a bridge's global stiffness and dynamic behavior. Based on the design drawings and field observations, the boundary conditions for Span 3 were modeled as follows:

- *East End Support:* This support was modeled as an idealized pinned connection, with all three translational degrees of freedom (x, y, and z) restrained, while allowing free rotation about all axes.
- *West End Support:* This support represents an expansion bearing. It was modeled with a combination of restraints and a spring element. The vertical (z-axis) and lateral (y-axis) translations were fully restrained. However, to represent the realistic, partial flexibility of the aged bearing in the longitudinal direction, a linear spring element was introduced to restrain motion along the bridge's longitudinal axis (x-axis). The initial stiffness of this spring was estimated and later treated as a key uncertain parameter for calibration.

Connections between the truss members at the panel points, which are physically made with large, riveted gusset plates, were simplified in the model. All intersecting members at a joint were connected to a single, shared node. This idealization treats the connections as fully rigid, which is a common and computationally efficient assumption for the global analysis of truss bridges.

3.4 Simulation of Moving Train Loads

To validate the model against the measured deflection data, it was necessary to simulate the live load imposed by the passing trains. A full vehicle-bridge interaction analysis can be computationally intensive. Therefore, a simplified yet effective approach was adopted to represent the moving train loads. The series of axles of a given train was modeled as a sequence of time-dependent, triangular pulse loads applied at the nodes along the rails of the FE model [16,17].
Each of the train's wheel loads is represented as a triangular pulse load (Figure 8). This triangular shape assumes a linear variation of contact force over time at each node, which approximates the rising and falling nature of the dynamic wheel–rail interaction as the wheel approaches, crosses, and moves past a specific point on the bridge. It serves as a simplified yet effective representation of the transient loading behavior caused by moving axles [17]. The triangular profile also helps mitigate numerical instabilities during dynamic simulations, making it suitable for time–history analysis in finite element modeling [18]. The loads were moved forward from the west end of the bridge to the east end of the bridge over a total of 100 discrete steps. The loads were moved by 37.2 cm (14.7 in). The load time (t) is defined by dividing the distance between two consecutive nodes in the FE model of the rail (d) by the desired vehicle traveling speed (V). The integration time was defined in the software using the sub-steps of the load. Figure 8 illustrates the triangular time history of a moving wheel load, where the load increases from zero to a peak axle loading and then decreases to zero as the wheel crosses a point/node on the bridge.

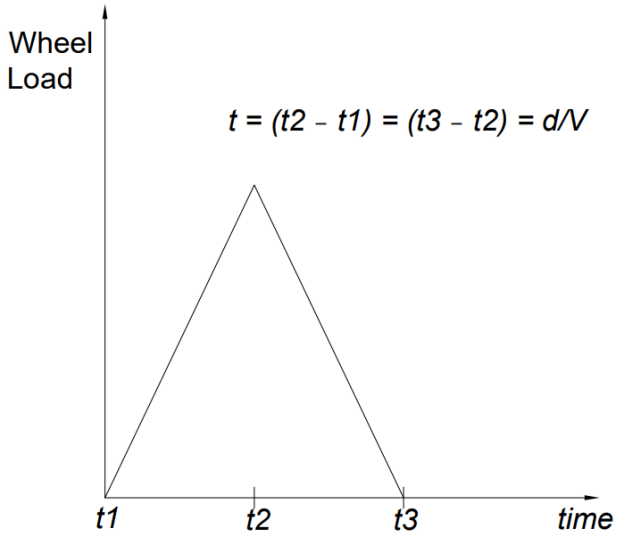

Figure 8: Triangular pulse load model of force applied in the finite element model.

For the preliminary analysis, the Metro-North M8 (MTNR M8) service loading (Figure 9a) is applied in the FE model. Each train's axle load time history was modeled as a triangular load (Figure 9b). The MTNR M8 is an electric multi-axle railroad car built by Kawasaki Rail Car, Inc., for exclusive use on the Metro-North Railroad New Haven Line and the CTrail Shoreline East. The train can reach a maximum speed of 161 km/h (100 mph) and an operational speed of 129 km/h (80 mph). The typical composition is four to five married (double) cars, each with the same axle load.

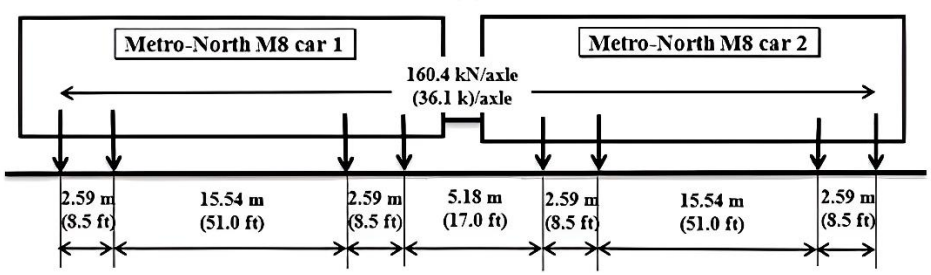

(a)

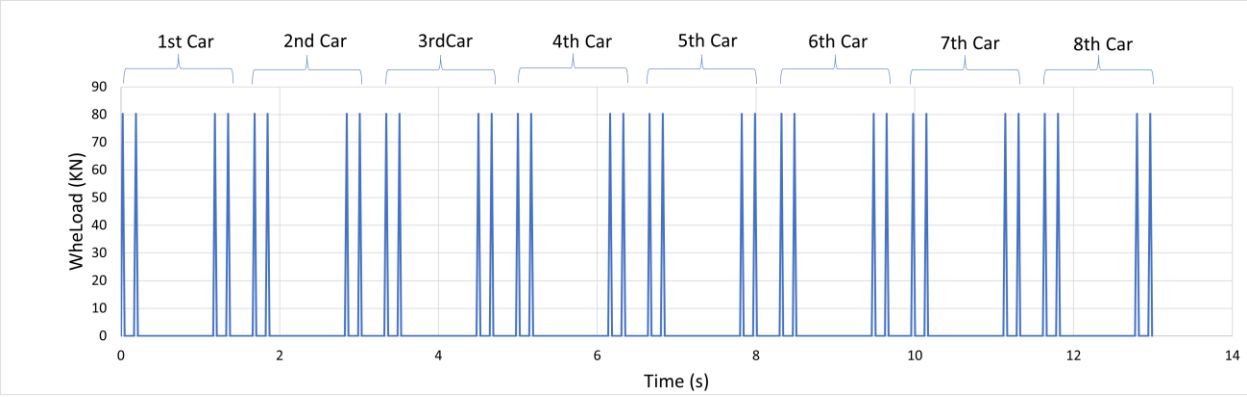

(b)

Figure 9: Metro-North M8 Train: (a) Axle loading, (b) Triangular pulse-shaped wheel loading applied in Finite Element (FE) model.

3.5 Initial Model Validation and Discrepancy Analysis

Before proceeding with the model updating process, the predictive capability of the initial, uncalibrated FE model was assessed. A dynamic time-history analysis was performed in ANSYS using the simulated Metro-North M8 train load. The resulting simulated peak vertical deflections and the model's natural frequencies (obtained from a modal analysis) were then directly compared with the corresponding values derived from the field test data.

The field test data from the LDV (and supplementary accelerometers) were processed to obtain time-domain deflection histories and frequency-domain spectra for span 3 of the Cos Cob Bridge. The Fast Fourier Transform (FFT) was applied to vibration data to identify the bridge's natural frequencies from the free vibration response obtained after train traversals. Table 4 compares the peak vertical deflections measured at mid-span (and other sensor locations) during the train tests with those obtained from the initial FE model simulation under similar loading conditions (same train type and speed). These initial comparisons help establish the baseline accuracy of the FE model prior to calibration.

Table 4: Comparison of FE Model Transient Vertical Peak Deflection and Field Test Results at Different Locations of the Cos Cob Bridge During MTNR M8 Train Traversal

Location	**FE Transient Vertical Deflection Results**$^{+}$	**Field Test Vertical Displacement Results**$^{+}$	**% Difference of FE Results with Respect to the Field Test Results**
Vib 1	−3.69 mm	−3.38 mm	9.17%
Vib 2	−3.43 mm	−3.04 mm	12.82%
Vib 3	−2.81 mm	−2.61 mm	7.66%

Note: $^{+}$The negative values in columns 2 and 3 represent the vertical downward deflection of the bridge.

As shown in Table 3, the initial FE model predicted slightly larger deflections than those observed in the field. The errors ranged from about 7.7% to 12.8%, with the largest discrepancy at the Vib 2 location. These differences, while not enormous, are significant in the context of model validation, and they motivated the subsequent model updating process.

The field vibration data also revealed the bridge's natural frequencies during free vibration (i.e., after the train had moved off the span). Table 5 presents the first three natural frequencies identified from the field measurements (for lateral and vertical modes), after the MTNR M8 train traversal. These frequencies were identified using data collected from three different sensor locations: Vib 1, Vib 2, and Vib 3. The frequency values extracted across all sensor locations are very close to each other, indicating that sensor placement had a minimal impact on the results. Figure 10 illustrates the typical frequency spectrum obtained from the LDV data, where peaks corresponding to the bridge's modal frequencies can be observed.

Table 5: Natural Frequencies of the Cos Cob Bridge During Free Vibration after MTNR M8 Train Traversal

Mode	Natural Frequency (Hz)			Initial FE Results (Hz)
	Vib 1	Vib 2	Vib 3	
1st Lateral	3.22	3.28	3.31	3.79
2nd Lateral	8.51	8.56	8.59	8.69
1st Vertical	7.56	7.61	7.65	8.25

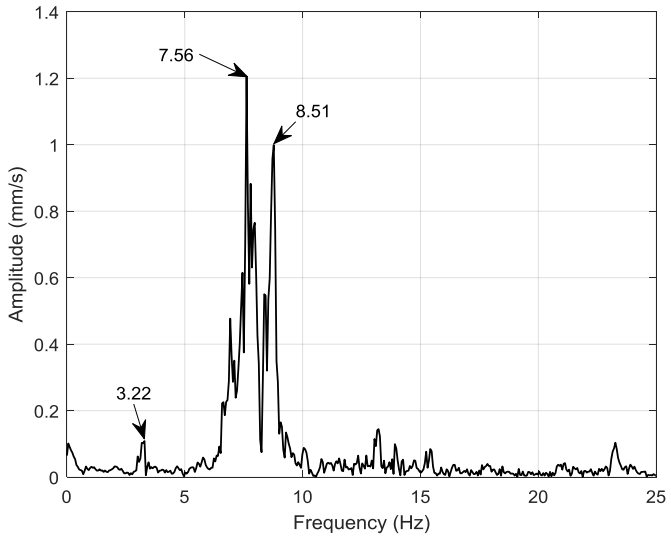

Figure 10: Typical Natural frequency of the Cos Cob Bridge during free vibration after Metro-North M8 train traversal.

The initial FE model's natural frequency predictions were close but not identical to the measured values. For example, the initial model gave a first lateral mode around 3.79 Hz and a first vertical mode around 8.25 Hz, indicating the model was somewhat stiffer than the actual structure (predicting higher frequencies). The second lateral mode from the model was around 8.69 Hz, similarly higher than measured.

In the initial FE model analysis, the simulated vertical displacement was found to be higher than the displacement measured from the field test, indicating that the model was initially less stiff under dynamic loading. At the same time, the natural frequencies of the model were higher than those observed natural frequencies in the field, which typically indicates a stiffer structural behavior in terms of dynamic characteristics. Due to these contradictions, it is important to perform model updating.

Chapter 4: Model Updating, its Results, and Load Rating

4.1 Identification and Parameterization of Uncertain Variables

The first step in the model updating process is to identify the parameters within the FE model that are both uncertain and have a significant impact on the structural responses of interest (i.e., deflections and natural frequencies). Based on the initial discrepancy analysis, literature review, and established engineering judgement regarding historic steel structures, four parameters were selected for calibration:

1. *Young's Modulus (E) of Steel:* To account for material variability, long-term degradation effects, and residual stresses, the modulus of elasticity for all steel truss members was treated as an uncertain variable. It was allowed to vary within a plausible range of ±5% of its nominal value of 2.0×10^{11} Pa.
2. *Density (ρ) of Steel:* While the density of steel is generally well-defined, this parameter was varied to implicitly account for additional mass on the structure that was not explicitly modeled. This includes non-structural components such as fasteners, gusset plates, instrumentation cables, and other elements added during the bridge's long service life. The parameter was allowed to vary between 7000 and 8100 kg/m³.
3. *Cross-Sectional Area Reduction:* To represent potential section loss due to corrosion or rivet slip, a uniform reduction factor was applied to the cross-sectional areas of all steel members. Based on the visual observation during the site visit and the prior inspection report [15], a maximum cross-sectional area reduction limit of 10% was selected. The reduction factor represents the worst-case cross-sectional deterioration identified and was used as an upper bound for the sensitivity analysis. A negative percentage change indicates a reduction of the nominal cross-sectional area. For example, a −6% change means the member cross-sectional areas are 94% of their original values.
4. *Support Spring Stiffness (k):* The longitudinal spring at the west-end support simulates translational flexibility, unlike a pinned support that restrains all translations but allows rotations. The stiffness was varied between 50,000 and 250,000 N/mm. The range was determined by comparing vertical displacements from the FEM under two boundary conditions: pinned-roller and fully pinned. The lower bound produced displacement similar to the pinned-roller case, while the upper bound matched the fully pinned condition. This parameter was treated as uncertain and sampled using a log-normal distribution. A similar approach to modeling support flexibility through spring stiffness was adopted by Svendsen et al. [19] in their sensitivity-based bridge model updating.

These four parameters formed the vector of updating variables, $\theta = \{E, \rho, A\%, k\}$ which the optimization algorithm would seek to refine.

4.2 Model Updating and Calibration

Using the procedure outlined in Chapter 2, comprehensive sensitivity analysis and optimization were conducted to calibrate the FE model. The analysis confirmed that the parameters identified (modulus of elasticity of steel, density of steel, cross-sectional area reduction, and support spring stiffness) had the most significant impacts on the outputs of interest (vertical deflections and

frequencies). By integrating an initial broad exploration of the parameter space (via log-normal sampling of the parameters) with the focused optimization of the genetic algorithm, this study efficiently calibrated the model to reflect the real-world behavior of the bridge. The GA's evolution of the parameter set is illustrated in Figure 11, which plots the fitness function (inversely related to Φ) versus the number of iterations; the curve shows a clear convergence toward an optimal solution. Individual sensitivity curves were not developed in this study, as all parameters were varied simultaneously using a genetic-algorithm-based optimization approach, making it difficult to isolate the effect of a single variable. These curves typically illustrate how a response changes when one parameter varies while others are held constant. Future work may consider one-variable-at-a-time studies to generate such curves and better quantify parameter influence.

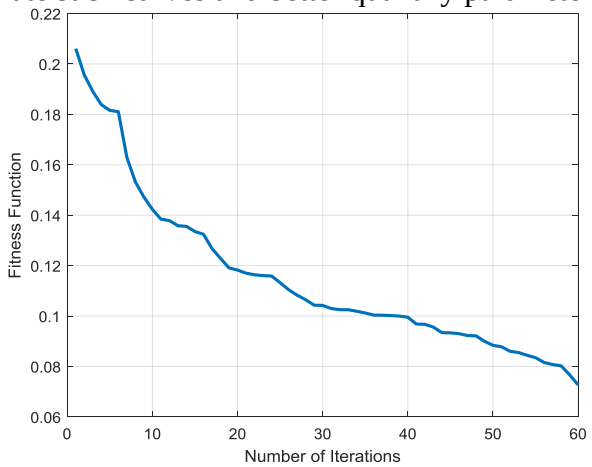

Figure 11: Fitness function vs. number of iterations

Through the sensitivity analysis and GA optimization, the model calibration homed in on a specific set of parameter values that produced the best agreement with the field data. The MATLAB code to generate the optimized parameters is presented in Appendix D. These optimized parameters were as follows:

- Young's modulus (E): 1.918×10^{11} Pa. This value is about 4% lower than the nominal 2.0×10^{11} Pa for steel, suggesting a slight reduction in effective stiffness of the structure. The reduction plausibly reflects the effects of long-term material degradation, residual stresses, and non-ideal boundary/support or connection behavior in the century-old Cos Cob Bridge. Factors such as fatigue damage, micro-cracking, and riveted joints may contribute to a slight reduction in the effective stiffness of the structure.
- Density (ρ): 8100 kg/m^3. This is higher than the typical steel density of 7850 kg/m^3, possibly accounting for additional structural and non-structural mass in the system (for instance, track, fasteners, and other non-structural attachments like electrical components not explicitly modeled). This calibration adjustment effectively lowers the model's natural frequencies, aligning better with field-measured responses.
- Cross-sectional area change (A%): −6.23%. A small uniform reduction (around 6%) in the cross-sectional areas of members improved the match with observed deflections, consistent with minor section losses from corrosion over time, especially in weather-exposed regions, or an overestimation of section sizes in the original as-built documentation. It may also capture unmodeled eccentricities or fabrication tolerances that reduce effective member stiffness.

- Longitudinal stiffness (k at support): 1.6493×10^5 N/mm. This value represents the optimized stiffness of the west-end support. It indicates that the support is not completely rigid longitudinally; the optimized stiffness suggests a partially flexible support that allows a small amount of movement. This flexibility can occur due to bearing play or deformation of support elements, and adjusting this parameter was important to match the measured deflection and vibration characteristics.

These parameters were obtained through the GA and then input into the ANSYS FE model for verification. With the updated parameters, the FE model was re-run to predict the bridge's response under the same loading scenarios as the field tests.

4.3 Updated FE Model

Following the sensitivity analysis and GA optimization, the FE model of the Cos Cob Bridge was updated with the optimized parameter values listed above. The final step was to compare the updated model's responses against the field measurements (and against the initial model results) to quantify the improvements achieved through calibration.
The primary focus was on the vertical deflection responses at the three instrumented locations (Vib 1, Vib 2, Vib 3) under the crossing of a Metro-North M8 train, as this scenario was used to drive the optimization. Table 6 presents the peak vertical deflections at those locations from the field test, the initial FE model, and the updated FE model for the M8 train case. Figure 12 (a-c) provides the full time-history curves of vertical deflection at Vib 1, Vib 2, and Vib 3 from both the field test and the updated FE model (showing a close overlap).

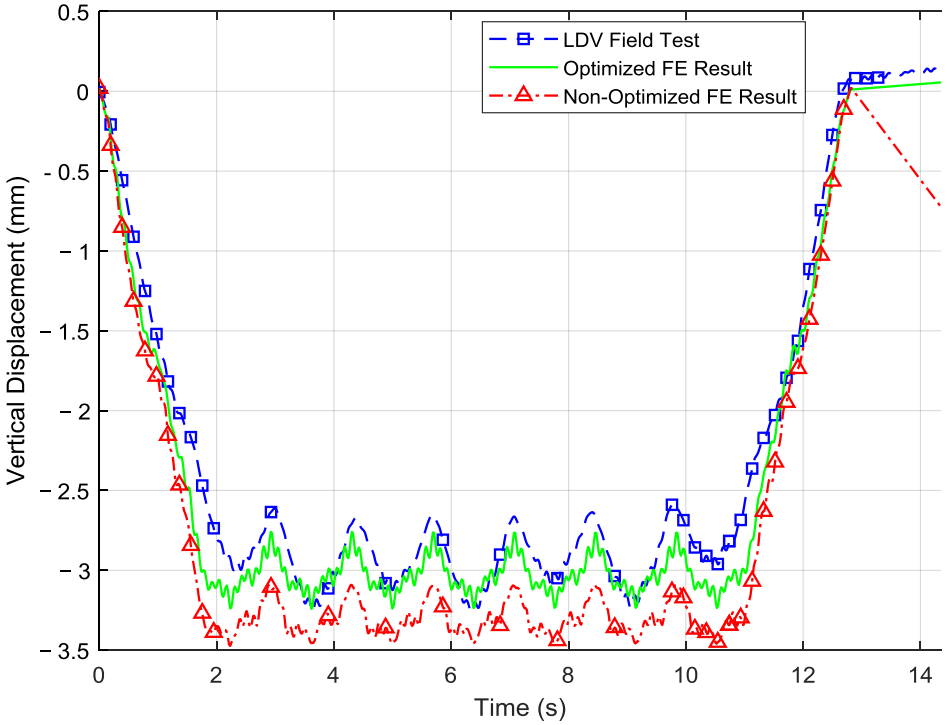

(a)

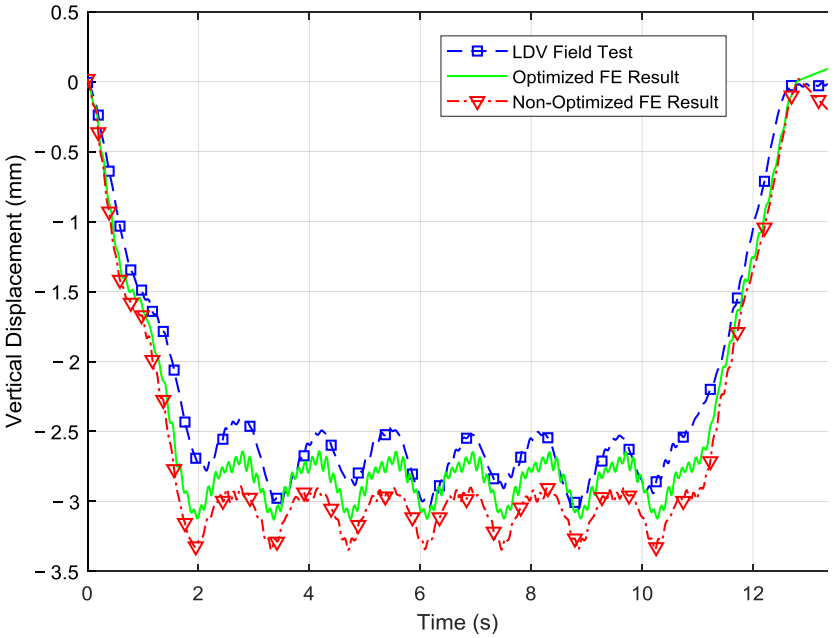

(b)

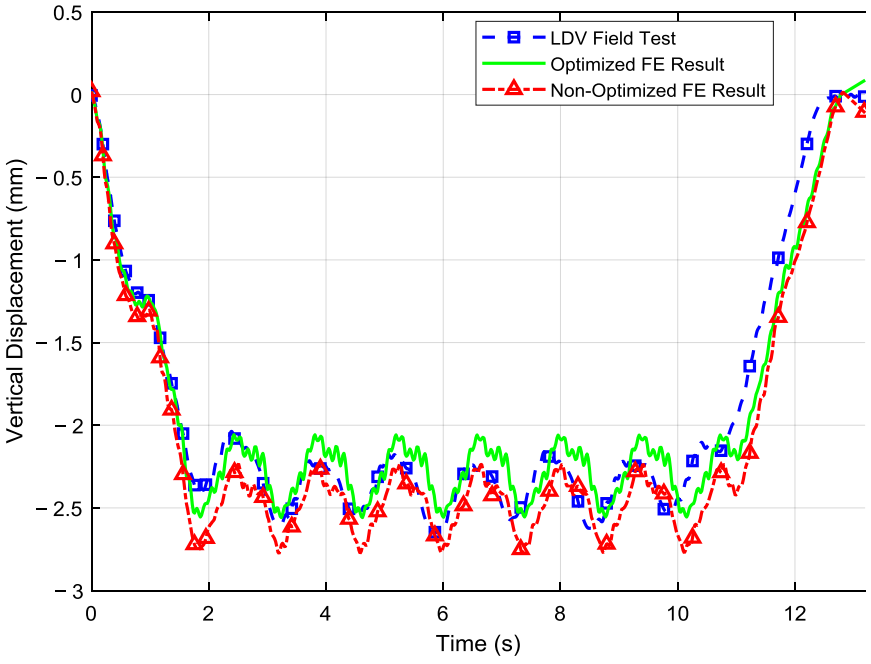

(c)

Figure 12: Vertical displacement results of the Cos Cob Bridge under MTNR M8 train loading at (a) Vib 1 @ 64 kmph, (b) Vib 2 @ 58 kmph, and (c) Vib 3 @ 53 kmph.

Table 6: Comparison of Peak Vertical Deflection Results of the Cos Cob Bridge between Field Test, Initial FE Model, and Optimized FE Model under Different Train Loadings

Train Type	Location	Field Test Max Deflection (mm)$^{+}$	Initial FE Max. Deflection (mm)$^{+}$*	Updated FE Max Deflection (mm)$^{+}$*
Metro North M8	Vib 1	−3.38	−3.69 (9.17%)	−3.24 (4.14%)
	Vib 2	−3.04	−3.43 (12.82%)	−3.13 (2.96%)
	Vib 3	−2.61	−2.81 (7.66%)	−2.58 (1.14%)
AMTRAK Acela	Vib 2	−4.581	−6.131 (33.835%)	−5.191 (13.315%)
AMTRK Regional	Vib 2	−4.413	−5.889 (33.446%)	−4.841(9.698%)

Note: $^{+}$The negative values in columns 3, 4, and 5 represent the vertical downward deflection of the bridge.

*The percentage shown in columns 4 and 5 represents the percentage difference of the FE model predictions (initial and updated) with respect to the field test max. deflection values.

As shown in Table 5, the updated FE model's deflection predictions exhibit a marked improvement over the initial model at various locations and train speeds. For the M8 train, the initial model over-predicted the deflection at Vib 2 by about 12.8%, whereas the updated model's prediction is within 3% of the measured value. Similar improvements were observed at Vib 1 and Vib 3: the initial errors of 9.2% and 7.7% were reduced to about 4.1% and 1.1%, respectively. The direction of correction is consistent—the initial model was generally too flexible (producing larger deflections than measured), and the optimization increased the stiffness of the updated FE model, such that deflections decreased with respect to the initial model, and matched the field values more closely. Figure 16 (a–c) illustrates these comparisons graphically for the M8 train case at three different locations, with the updated model's deflection curves nearly overlapping the field curves.

After confirming the updated model's accuracy for the M8 loading (which was used for calibration), the model was further validated using the two Amtrak train cases (Amtrak Regional and Acela Express) that were also recorded during field testing. These cases serve as independent checks because they involve different total loads, axle spacing, and speeds. The updated model was subjected to the Amtrak Regional and Acela load cases (using the same calibrated/updated parameters, with the only difference being the loading inputs). Figure 13(a, b) shows the axle load configurations for the Amtrak Regional and Acela trains that were used in the analysis. The results, included in Table 5 for Vib 2, show that the updated model also performed well for these scenarios. For the Amtrak Acela (a high-speed trainset with a different axle configuration), the initial model's peak deflection error at mid-span was quite large (~33.8%), whereas the updated model cut that error to about 13.3%. For the Amtrak Regional locomotive, the error dropped from ~33.4% to ~9.7% after calibration/optimization. The larger initial errors for the Amtrak trains suggest that the initial model's assumptions (especially regarding dynamic amplification or support stiffness)

might not have been adequate for heavier or faster trains, but the updated model, calibrated primarily on the M8 data, generalized well to these cases. Figure 14 (a, b) compares the updated FE model and field deflection time histories at Vib 2 for those trains. The updated model captures the peak deflections and overall response shape reasonably well for both train loading cases.

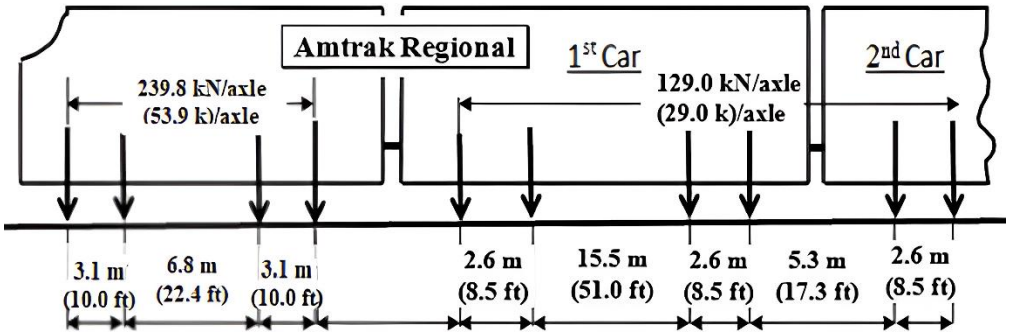

(a)

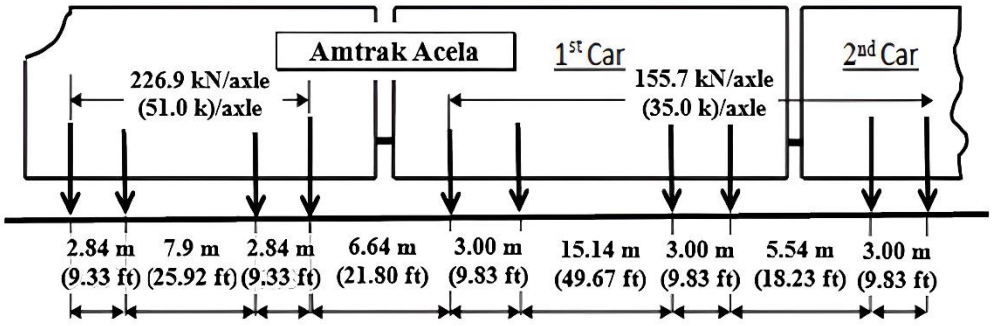

(b)

Figure 13: Axle loading for Finite Element Modeling of (a) Amtrak Regional Train, (b) Amtrak Acela Train *[20]*.

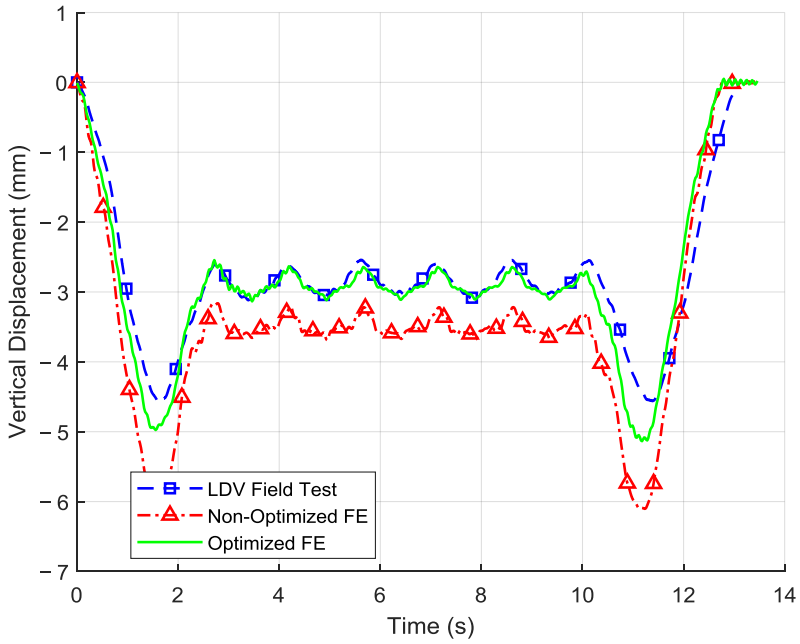

(a)

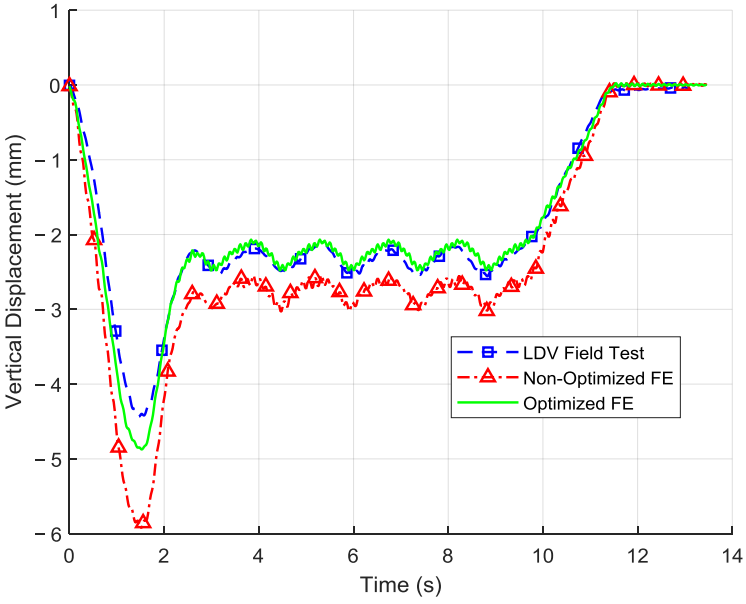

(b)

Figure 14: Vertical displacement results of Cos Cob Bridge under (a) Amtrak Acela Train at Vib 2 @ 64 kmph and (b) Amtrak Regional Train at Vib 2 @ 64 kmph.

In addition to deflections, the first few natural frequencies of the updated FE model were computed and compared to the field-identified values (from Table 4). Table 7 summarizes the comparison of the three primary modal frequencies before and after model updating. The initial FE model

frequencies are included along with the percentage errors relative to the field values, and the same is performed for the updated model frequencies. The updated model frequencies show much smaller errors, indicating that the model's dynamic characteristics have been successfully tuned.

Table 7: Comparison Table of Natural Frequencies of the Cos Cob Bridge.

Mode	Natural Frequency (Hz)				
	Field Test	**Initial FE Result**	**% Difference***	**Optimized FE Result**	**% Difference***
1st Lateral	3.22	3.79	17.70	3.31	2.795
2nd Lateral	8.51	8.69	2.12	8.43	−0.940
1st Vertical	7.56	8.25	9.13	7.78	2.910

Note: *Column 4 represents the % difference value of the initial FE result with respect to the field test, and Column 6 represents the % difference value of the optimized FE result with respect to the field test. And a negative sign in Column 6 indicates that the FE result is less than the field test result.

The improvement in frequency prediction can be attributed to the adjustments in E (reducing stiffness) and ρ (increasing mass) in the calibration process. The slightly increased density used in the model is justified by the cumulative mass of structural and non-structural components not explicitly captured in the model. These include fasteners, rivets, gusset plates, instrumentation cables, and additional steel components likely added during the rehabilitation process over the years. The close agreement across both lateral and vertical modes suggests that the calibration did not over-fit to just one mode but rather achieved a balanced adjustment that benefits the overall dynamic behavior.

After the model updating process, the vertical displacement predictions of the updated model are higher, in general, than the corresponding field test results, and the natural frequency predictions of the updated model are also higher, in general, than the corresponding field test-based estimates. In the case of vertical displacements, the updated bridge model is less stiff, but in the case of natural frequencies, the updated bridge model is stiffer than the present condition of the actual bridge. This apparent contradiction arises because the structure's responses are influenced by different aspects of structural stiffness and mass distribution. The overestimated displacement may be due to simplified boundary conditions or idealized material properties. On the other hand, the higher natural frequencies could be due to underestimation of system mass, exclusion of non-structural components like track fixity, or overly rigid connections modeled in the FE analysis. These discrepancies highlight the need for model updating to accurately reflect the bridge's actual dynamic response.

The results of this study confirm the effectiveness of the proposed updating method. Unlike the digital twin approaches by Lai et al. [21], which use continuous SHM data for Bayesian forecasting, and Nhamage et al. [22], which combine BIM and real-time fatigue simulation, this study achieves similar accuracy through a simpler, data-sparse approach. While those methods offer predictive capabilities and detailed visualization, our results show that reliable model calibration is still possible without continuous monitoring, making it well-suited for aging bridges with limited instrumentation.

Overall, the updated FE model of the Cos Cob Bridge shows significantly better agreement with real behavior, both in vertical displacement during train passage and in free vibration characteristics, compared to the initial model. These improvements validate the effectiveness of the sensitivity-driven, GA-based updating framework in aligning simulated and observed bridge responses. The calibrated and updated model can now be used with more confidence for further analysis, such as fatigue life estimation, load rating under various train loadings, or studying the effects of hypothetical strengthening or deterioration scenarios.

4.4 Overview of AREMA Load Rating

The load rating of the Cos Cob bridge was conducted using the AREMA Manual for Railway Engineering 2015 [23]. As discussed in Chapter 2, the AREMA Manual specifies two distinct load rating levels, Normal Rating (day-to-day permissible loads) and Maximum Rating (occasional loads), for the bridge. Section 4.4.1 summarizes the calculated allowable stresses for bending and shear for normal and maximum rating of the bridge members.

4.4.1 Calculated Allowable Stresses for Normal and Maximum Rating

The calculations of allowable bending and shear stresses are expressed in terms of the minimum yield strength of the material of the bridge members. AREMA 2015 Chapter 15, Section 7.3.3.3.a, suggests that "in the absence of test records, the material yield strength shall be taken as 30 ksi for open-hearth steels (including A7)." Track 4 of the Cos Cob Bridge was determined to be made from A7 steel. So, for the rating purpose, the yield strength (f_y) was taken as 30 ksi. The calculated allowable stresses for normal and maximum rating are presented in Table 8 below.

Table 8: Calculated Allowable Stresses for Normal and Maximum Rating

Stress Type	**Normal Rating**	**Maximum Rating**
Flexural Tension	16.5 ksi	24 ksi
Flexural Compression	16.5 ksi	24 ksi
Shear	10.5 ksi	18 ksi

4.5 Load Rating Procedure using the Updated FE Model

The final calibrated and updated FE model (described previously in Sections 4.2 and 4.3) was used as the computational tool for the load rating. The use of the updated model ensures that the calculated member forces reflect the true load distribution and behavior of the bridge to a high degree of accuracy. While the Cooper E80 rating provides a standardized measure of the bridge

members' capacities, it is also important for the bridge owners to know the specific capacity for the actual trains that operate regularly on the bridge. Therefore, in addition to the Cooper E80 analysis, the load rating was also performed under the MTNR M8, AMTRAK Regional, and AMTRAK Acela trains. The maximum bending and shear stresses for each bridge member under different train loading conditions extracted from ANSYS were input into MS-EXCEL spreadsheets to calculate the ratings for bridge members. Table 9 presents the maximum bending stress and shear stress in the members of the bridge under different train loadings.

Table 9: Summary of Maximum Bending Stress and Shear Stress of the Cos Cob Bridge Members

Members	Cooper E 80		MTNR M8		Amtrak Regional		Amtrak Acela	
	Max. Bending Stress (ksi)	Max. Shear Stress (ksi)	Max. Bending Stress (ksi)	Max. Shear Stress (ksi)	Max. Bending Stress (ksi)	Max. Shear Stress (ksi)	Max. Bending Stress (ksi)	Max. Shear Stress (ksi)
U0U2	7.8	14	1.8	3.7	2.7	5.9	2.6	5.8
U2U4	4.2	28.8	1.1	6.3	1.6	9.2	1.5	9.2
U4U6	3.2	14.2	0.9	3.4	1.3	4.9	1.3	4.9
U6U8	3.2	12.9	0.8	3	1.3	4.4	1.3	4.4
L0L2	1.7	7.2	0.4	0.5	0.4	0.6	0.5	0.6
L2L4	0.7	1.1	0.2	0.3	0.2	0.3	0.2	0.3
L4L6	3	3.2	0.8	0.7	1	1	1.1	1
L6L8	2.7	3.2	0.7	0.7	0.9	1	0.8	1

4.6 Rating Analysis Results

The rating of the bridge members was calculated using MS Excel spreadsheets the procedure outlined in the AREMA manual Chapter 15 as described in Section 2.4. Tables 10 and 11 present the bridge normal rating and the maximum rating, respectively, of the bridge members at 60 mph.

Table 10: Normal Rating of the Bridge Members Under Different Train Loadings

Members	Cooper E 80		MTNR M8		Amtrak Regional		Amtrak Acela	
	Normal Bending Rating	Normal Shear Rating	Normal Bending Rating	Normal Shear Rating	Normal Bending Rating	Normal Shear Rating	Normal Bending Rating	Normal Shear Rating
U0U2	2.1	1.2	9.2	2.8	6.1	1.8	6.3	1.8
U2U4	3.9	0.4	15.0	1.7	10.3	1.1	11.0	1.1
U4U6	5.2	0.7	18.3	3.1	12.7	2.1	12.7	2.1
U6U8	5.2	0.8	20.6	3.5	12.7	2.4	12.7	2.4
L0L2	9.7	1.5	41.3	21.0	41.3	17.5	33.0	17.5
L2L4	23.6	9.5	82.5	35.0	82.5	35.0	82.5	35.0
L4L6	5.5	3.3	20.6	15.0	16.5	10.5	15.0	10.5
L6L8	6.1	3.3	23.6	15.0	18.3	10.5	20.6	10.5

Table 11: Maximum Rating of the Bridge Members Under Different Train Loadings

Members	Cooper E 80		MTNR M8		Amtrak Regional		Amtrak Acela	
	Max. Bending Rating	Max. Shear Rating	Max. Bending Rating	Max. Shear Rating	Max. Bending Rating	Max. Shear Rating	Max. Bending Rating	Max. Shear Rating
U0U2	3.1	1.7	13.3	4.9	8.9	3.1	9.2	3.1
U2U4	5.7	0.6	21.8	2.9	15.0	2.0	16.0	2.0
U4U6	7.5	1.3	26.7	5.3	18.5	3.7	18.5	3.7
U6U8	7.5	1.4	30.0	6.0	18.5	4.1	18.5	4.1
L0L2	14.1	2.5	60.0	36.0	60.0	30.0	48.0	30.0
L2L4	34.3	16.4	120.0	60.0	120.0	60.0	120.0	60.0
L4L6	8.0	5.6	30.0	25.7	24.0	18.0	21.8	18.0
L6L8	8.9	5.6	34.3	25.7	26.7	18.0	30.0	18.0

As presented in Table 10, the normal rating factors for members U2U4, U4U6, and U6U8 were found to be below 1.0, indicating insufficient capacity for unrestricted service under typical rating assumptions. Additionally, Table 11 shows that the maximum shear rating factor for U2U4 remains below 1.0 under Cooper E-80 loading, which implies that these members are overstressed even under ideal load positioning and structural conditions. Conversely, for the Metro-North M8, AMTRAK Regional, and Acela train loadings, all considered members demonstrated rating factors greater than 1.0, confirming the adequacy of the bridge for current passenger service demands.

Chapter 5: Summary, Conclusion, and Recommendations

This chapter summarizes and draws conclusions from the key findings of the following components of the project: field testing and initial FE model validation, subsequent model updating, and load rating analysis. Additionally, the study's limitations are discussed and recommendations are made for future work. The final section also evaluates how well the research objectives were met, and what the results mean for the specific bridge studied (Cos Cob Bridge).

5.1 Summary

This research presented a comprehensive approach for evaluating a century-old steel truss railroad bridge by combining field testing, finite element modeling, and model updating using sensitivity analysis and optimization techniques. Field-measured responses were used to calibrate the key parameters through a Real-Coded Genetic Algorithm to accurately represent the responses of the bridge, and the updated model was used to perform a load rating analysis of the bridge according to the AREMA manual (AREMA 2015).

5.2 Conclusions

- *Field Testing and Initial FE Modeling*

A primary finding was the significant discrepancy between the bridge's observed behavior and the predictions of the initial FE model. Under the MTNR M8 train loading, the initial FE model vertical displacement results at three different locations were higher (7%-12%) than the measured field test results. Similarly, the natural frequencies from the initial FE model for different modes were higher (2%-17%) than the measured natural frequencies. Interestingly, these discrepancies were even more pronounced under heavier train loads like Amtrak Regional, where the initial model's deflection predictions were off by as much as 33%. In all cases, the FE model overestimated the vertical displacements and natural frequencies, indicating differences in stiffness, mass representation, and boundary conditions. These differences confirmed that the bridge's properties have changed after a century of service, highlighting the necessity of calibrating models with real-world data to ensure accurate safety assessments.

- *Optimized Structural Parameters and Updated FE Model*

To accurately represent the bridge's current condition, the model was updated by changing the values of four parameters: Young's modulus, density, cross-sectional area of members, and boundary condition stiffness (i.e., support stiffness). The final values for the parameters selected by the Genetic Algorithm provide valuable physical insights into the as-is condition of the historic bridge: (1) *Young's Modulus (E) of* 1.918×10^{11} Pa is approximately 4% lower than the nominal value for steel, indicating slight stiffness reduction, (2) *Density (ρ)* of 8100 kg/m³ is slightly higher than the typical value for steel (7850 kg/m³), capturing additional non-structural mass, (3) a -6.23% *cross-sectional area* change represents a small, uniform reduction in the cross-sectional area of the steel members with minor corrosion, and (4) a *Longitudinal Stiffness (k at support*) of 1.6493×10^{5} N/mm representing partial bearing restraint. The calibrated FE model, updated with these optimized parameters, demonstrated a significant

improvement in predictive accuracy. Peak deflection differences with respect to the field test were reduced to a range of 1–14%, and natural frequency differences with respect to the field test were reduced to below 3% across the primary modes of vibration.

- *Load Rating*

The load rating analysis, which was performed using the calibrated and updated model, revealed a comprehensive assessment of the bridge's structural capacity. For the current operating passenger trains (i.e., Metro-North M8, AMTRAK Regional, and AMTRAK Acela passenger train loadings), all key structural members demonstrated rating factors greater than 1.0, indicating the bridge, in its current condition, is structurally adequate for these passenger train loadings.

However, the assessment against the Cooper E-80 design loading, representative of heavy freight, identified critical deficiencies. Several upper chord members were found to possess rating factors below 1.0, signifying that these members would be overstressed under such loading conditions. This outcome implies that the bridge lacks the capacity for unrestricted heavy freight service, a finding that aligns with the operational restrictions commonly placed on aging infrastructure of this type.

5.3 Limitations of the Study

While the results are largely positive, it is important to acknowledge the following limitations of the study: (1) The model was updated using only global field data, specifically overall deflection and natural frequencies. Therefore, the model should be used to assess the overall performance of the bridge, but it is not suitable for local analyses, such as stress concentration assessments. (2) The effectiveness of the Genetic Algorithm (GA) is limited by the completeness of the model itself. The optimization only adjusts existing parameters and cannot account for physical behaviors that were omitted from the model. For instance, if certain stiffness-contributing features are not included in the FE modeling, the GA might mask this by incorrectly altering other parameters to match the field data. We believe this risk is low in the present study, as our model was comprehensive and included all major components, such as the rails and ties. (3) The model's calibration is also limited by environmental factors, as all data were collected on a single day. Temperature can alter structural behavior, for instance, by causing support bearings to "lock up" in extreme cold, which would change the bridge's stiffness. Therefore, the model is validated only for the mild conditions on the test day, and its predictions may be less accurate during periods of extreme heat or cold. Despite these limitations, the high degree of predictive accuracy demonstrated by the updated model in multiple loading scenarios generates confidence in the overall quality of the model, indicating that it provides a robust representation of the current structural condition and behavior of the bridge.

5.4 Recommendations

While this study successfully achieved its objectives, it also highlighted some important limitations, as noted above. These limitations may serve as indicators of areas in which further research could enhance the methodology and broaden its applicability. The following recommendations are proposed for future work:

- *Enhanced Field Testing:* Future studies should consider employing a denser array of sensors, such as multiple LDVs or a scanning LDV system. This would allow for the capture of detailed, high-resolution mode shapes, which could then be incorporated as an additional target in the GA objective function. This would provide more spatial information for the calibration process, leading to an even higher level of model fidelity and better localization of stiffness or mass discrepancies.
- *Material and Connection Non-Linearities:* The current model utilizes linear-elastic material properties and simplified connections. Future research could incorporate more advanced modeling techniques, such as non-linear material models to capture plastic behavior under extreme loads, and the use of contact or non-linear spring elements to more accurately represent the behavior of riveted connections and bearings. This would be particularly valuable for ultimate capacity analysis and seismic assessment. However, a model that incorporates such nonlinearities will increase the computational cost and time.
- *Refinement of Boundary Conditions:* The current model employs idealized support representations. Future work could aim to more realistically replicate actual boundary conditions and support behavior, particularly the interactions at bearings and expansion joints. Using field instrumentation to capture boundary/support displacements can help validate and refine these assumptions.
- *Enhanced mass representation:* Additional mass from components such as fasteners, track fixity, and other non-structural elements were not explicitly modeled. Including these elements or applying an appropriate lumped mass correction can improve the accuracy of dynamic response prediction.

References

1. American Road & Transportation Builders Association. *2019 Bridge Report*; American Road & Transportation Builders Association: Washington, DC, USA, 2019. Available online: https://artbabridgereport.org/reports/2019-ARTBA-Bridge-Report.pdf (accessed on 15 July, 2025).
2. Witcher, T.R. From Disaster to Prevention: The Silver Bridge. *Civ. Eng.* **2017**, *87*, 44–47, doi:10.1061/ciegag.0001250.
3. Salem, H.; Helmy, H.; Fouly, A.E. Prediction of Bridge Behavior Through Failure: A Case Study Of The Minnesota I-35W Bridge Collapse. In Proceedings of the Structures Congress 2013; American Society of Civil Engineers: Pittsburgh, Pennsylvania, United States, April 30 2013; pp. 2904–2915.
4. Zhang, Y.; Zheng, K.; Heng, J.; Zhu, J. Corrosion-Fatigue Evaluation of Uncoated Weathering Steel Bridges. *Applied Sciences* **2019**, *9*, 3461, doi:10.3390/app9173461.
5. Spyrakos, C.C.; Raftoyiannis, I.G.; Ermopoulos, J.C. Condition Assessment and Retrofit of a Historic Steel-Truss Railway Bridge. *Journal of Constructional Steel Research* **2004**, *60*, 1213–1225, doi:10.1016/j.jcsr.2003.11.004.
6. Brownjohn, J.M.W. Structural Health Monitoring of Civil Infrastructure. *Phil. Trans. R. Soc. A.* **2007**, *365*, 589–622, doi:10.1098/rsta.2006.1925.
7. Khedmatgozar Dolati, S.S.; Caluk, N.; Mehrabi, A.; Khedmatgozar Dolati, S.S. Non-Destructive Testing Applications for Steel Bridges. *Applied Sciences* **2021**, *11*, 9757, doi:10.3390/app11209757.
8. Kaewunruen, S.; AbdelHadi, M.; Kongpuang, M.; Pansuk, W.; Remennikov, A.M. Digital Twins for Managing Railway Bridge Maintenance, Resilience, and Climate Change Adaptation. *Sensors* **2022**, *23*, 252, doi:10.3390/s23010252.
9. Armijo, A.; Zamora-Sánchez, D. Integration of Railway Bridge Structural Health Monitoring into the Internet of Things with a Digital Twin: A Case Study. *Sensors* **2024**, *24*, 2115, doi:10.3390/s24072115.
10. De Oliveira, C., Anand, R, Tripathi, S., and Malla, R. B. Structural Integrity, Safety, and Durability of Critical Members and Connections of Old Railroad Bridges under Dynamic Service Loads and Conditions; Final Report; Transportation Infrastructure Durability Center, U.S. Department of Transportation: Storrs, CT, USA, 2024 (Submitted).
11. Mottershead, J.E.; Link, M.; Friswell, M.I. The Sensitivity Method in Finite Element Model Updating: A Tutorial. *Mechanical Systems and Signal Processing* **2011**, *25*, 2275–2296, doi:10.1016/j.ymssp.2010.10.012.
12. Bathe, K.-J. Finite Element Procedures; Prentice Hall: Upper Saddle River, NJ, USA, 1996; ISBN 0-13-301458-4.
13. Farrar, C.R.; Worden, K. An Introduction to Structural Health Monitoring. *Phil. Trans. R. Soc. A.* **2007**, *365*, 303–315, doi:10.1098/rsta.2006.1928.
14. Malla, R.B.; de Oliveira, C.; Dhakal, S. Condition/Health Monitoring of Railroad Bridges for Structural Safety, Integrity, and Durability; Final Report; Transportation Infrastructure Durability Center, U.S. Department of Transportation: Storrs, CT, USA, 2022.
15. Underwater Construction. As-Built Drawings: Cos Cob Bridge No. 29.91, Rehabilitation of New Haven Line Movable Bridges Superstructure Repair; Metro-North Commuter Railroad Commuter Co. Connecticut Department of Transportation: Newington, CT, USA, 1990.

16. Anand, R., Dhakal, S., De Oliveira, C., and Malla, R. B. (2024). Displacement Response of a Truss-Type Steel Railroad Bridge during Train Passage. In *International Conference on Transportation and Development 2024* (pp. 680-687).
17. Anand, R.; Tripathi, S.; De Oliveira, C.C.; Malla, R.B. Field-Test-Driven Sensitivity Analysis and Model Updating of Aging Railroad Bridge Structures Using Genetic Algorithm Optimization Approach. *Infrastructures* **2025**, *10*, 195, doi:10.3390/infrastructures10080195.
18. Punetha, P.; Maharjan, K.; Nimbalkar, S. Finite Element Modeling of the Dynamic Response of Critical Zones in a Ballasted Railway Track. *Front. Built Environ.* **2021**, *7*, doi:10.3389/fbuil.2021.660292.
19. Svendsen, B.T.; Petersen, Ø.W.; Frøseth, G.T.; Rønnquist, A. Improved Finite Element Model Updating of a Full-Scale Steel Bridge Using Sensitivity Analysis. *Structure and Infrastructure Engineering* **2023**, *19*, 315–331, doi:10.1080/15732479.2021.1944227.
20. Jacobs, D.W.; Dhakal, S.; Malla, R.B. Live-Load Response of Eyebars on a 110-Year-Old Steel Truss Railroad Bridge. *Pract. Period. Struct. Des. Constr.* **2021**, *26*, 04020045, doi:10.1061/(ASCE)SC.1943-5576.0000523.
21. Lai, L.; Dong, Y.; Smyl, D. SHM-Informed Life-Cycle Intelligent Maintenance of Fatigue-Sensitive Detail Using Bayesian Forecasting and Markov Decision Process. *Structural Health Monitoring* **2024**, *23*, 187–210, doi:10.1177/14759217231160412.
22. Nhamage, I.; Dang, N.-S.; Horas, C.; Poças Martins, J.; Matos, J.; Calçada, R. Performing Fatigue State Characterization in Railway Steel Bridges Using Digital Twin Models. *Applied Sciences* **2023**, *13*, 6741, doi:10.3390/app13116741.
23. American Railway Engineering and Maintenance-of-Way Association (AREMA). *Manual for Railway Engineering*; AREMA: Lanham, MD, USA, 2014.

Appendix A: Cos Cob Bridge Members Cross Sections Assigned for FE Model

The cross sections of the Cos Cob Bridge members are shown below:

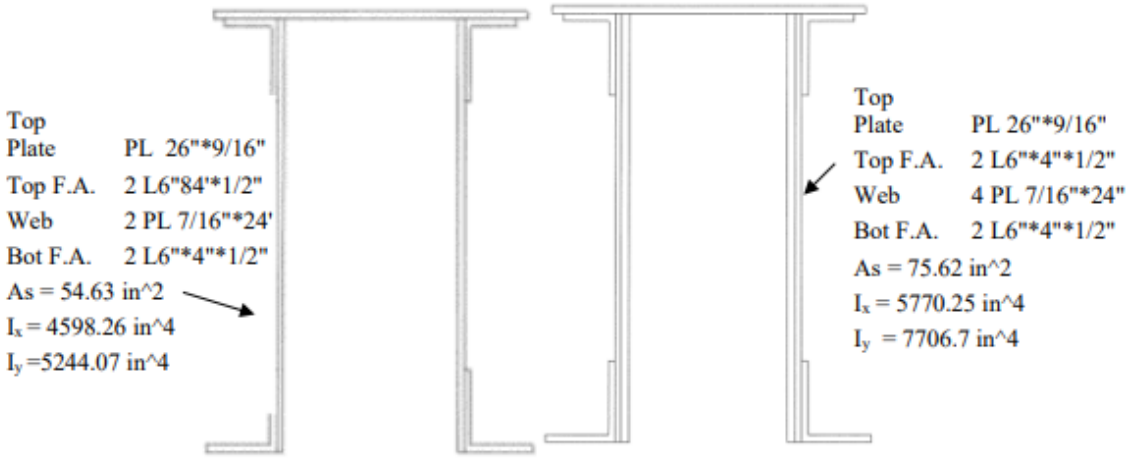

(a). Typical section; Node U0-U1, U7-U8 (Top Chord)

(b). Typical section; Node U1-U2, U6-U7 (Top Chord)

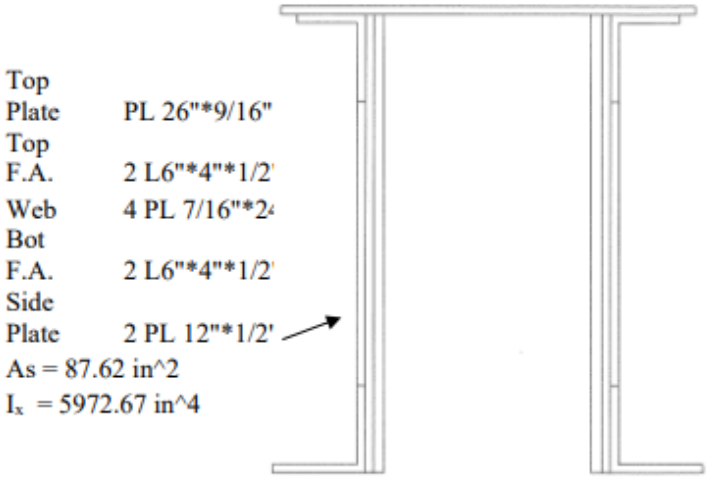

(c). Typical section; Node U2-U3, U5-U6 (Top Chord)

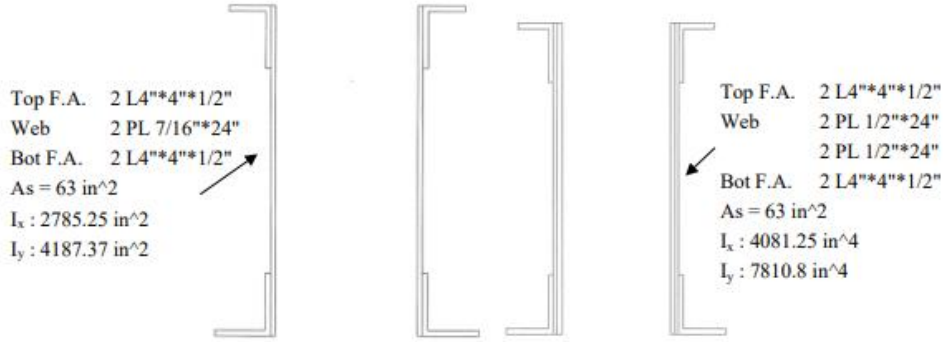

(d). Typical section; Node L0-L1, L7-L8 (Bottom Chord)

(e). Typical section; Node L1-L2, L6-L7 (Bottom Chord)

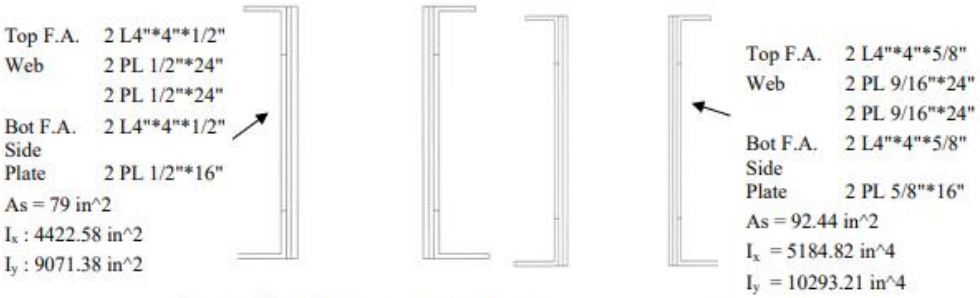

(f). Typical section; Node L2-L3 L5-L6 (Bottom Chord)

(g). Typical section; Node L3-L4, L4-L5 (Bottom Chord)

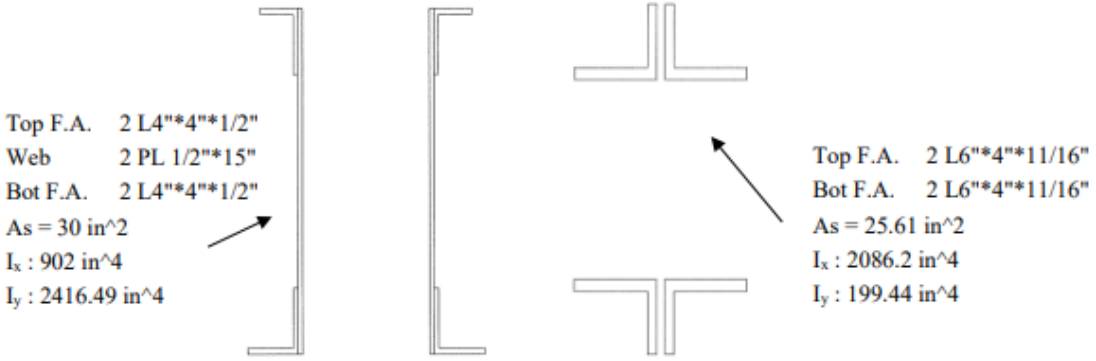

(h). Typical section; Node U0-L0, U8-L8 (End Post)

(i). Typical section; Node U2-L1 (Counters)

Appendix B: Genetic Algorithm MATLAB Code

The MATLAB code written to perform GA optimization is given below:

```
function run_ga_sensitivity_analysis

    % Ask if generating parameters for the first time
    first_run = input('Is this the first time generating parameters? (yes/no): ', 's');

    if strcmpi(first_run, 'yes')
        % Generate the first 12 sets of parameters using the specified ranges
        disp('Generating the first 12 sets of parameters within the given ranges...');
        parameters = generate_parameters();
        disp('Generated Parameters:');
        disp(parameters);

        % Save parameters to Excel for ANSYS input, starting at the second row
        writematrix(parameters, 'sensitivity_analysis_updated.xlsx', 'Sheet', '1st iteration values',
'Range', 'A2');
        disp('First 12 sets of parameters saved to "sensitivity_analysis_updated.xlsx" (Sheet: 1st
iteration values, starting at row 2).');

    elseif strcmpi(first_run, 'no')
        % Ask for the iteration number
        iteration_number = input('Which iteration are you running? (e.g., 2 for 2nd iteration): ');
        sheet_name = get_ordinal_suffix(iteration_number);

        % Check if this iteration has already been performed
        if ismember(sheet_name, sheetnames('sensitivity_analysis_updated.xlsx'))
            disp(['The iteration ', num2str(iteration_number), ' has already been done.']);
            % Automatically detect the next iteration
            next_iteration = iteration_number + 1;
            disp(['Proceeding to the next iteration: ', get_ordinal_suffix(next_iteration)]);
            sheet_name = get_ordinal_suffix(next_iteration);
        end

        % Retrieve previous results
        if iteration_number == 2
            % Generate new parameters for the second iteration using log-normal sampling
            disp('Generating new parameters for the 2nd iteration...');
            prev_sheet_name = get_ordinal_suffix(1);
            previous_parameters = readmatrix('sensitivity_analysis_updated.xlsx', 'Sheet',
prev_sheet_name, 'Range', 'A2');

            % Generate the second set of parameters using the same log-normal distribution
```

```
        parameters = generate_parameters();  % Generate fresh parameters within the given
ranges

        % Save the new parameters for the second iteration
        writematrix(parameters, 'sensitivity_analysis_updated.xlsx', 'Sheet', '2nd iteration values',
'Range', 'A2');
        disp('New parameters saved to "sensitivity_analysis_updated.xlsx" (Sheet: 2nd iteration
values).');

    elseif iteration_number >= 3
        % Retrieve all previous results
        disp('Retrieving parameters from all previous iterations...');
        previous_results = [];

        for i = 1:iteration_number-1
            prev_sheet_name = get_ordinal_suffix(i);
            results = readmatrix('sensitivity_analysis_updated.xlsx', 'Sheet', prev_sheet_name,
'Range', 'A2');
            previous_results = [previous_results; results]; % Append results from previous
iterations
        end

        % Sort based on fitness and create a new sheet for sorted data
        disp('Sorting parameters based on fitness for the GA process...');
        fitness = previous_results(:, end);  % Assuming fitness is in the last column
        [~, idx] = sort(fitness);

        % Sort all results based on fitness
        sorted_results = previous_results(idx, :);

        % Create a sheet name for sorted data from all previous iterations
        sorting_sheet_name = ['Sorted ', num2str(iteration_number-1), ' data'];
        writematrix(sorted_results, 'sensitivity_analysis_updated.xlsx', 'Sheet',
sorting_sheet_name, 'Range', 'A2');
        disp(['Sorted parameters from previous iterations saved to
"sensitivity_analysis_updated.xlsx" (Sheet: ', sorting_sheet_name, ').']);

        % Select the 12 smallest sets of parameters
        top_parameters = sorted_results(1:12, 1:4);

        % Generate the next set of parameters using a GA-inspired approach
        disp(['Generating new parameters for iteration ', num2str(iteration_number), ' using GA
approach...']);
        parameters = generate_ga_parameters(top_parameters);

        % Save the new parameters for the current iteration
```

```
        writematrix(parameters, 'sensitivity_analysis_updated.xlsx', 'Sheet', sheet_name, 'Range',
'A2');
        disp(['New parameters saved to "sensitivity_analysis_updated.xlsx" (Sheet: ',
sheet_name, ').']);
    end
  else
    disp('Invalid input. Please enter "yes" or "no".');
  end
end

% Function to generate ordinal suffixes (1st, 2nd, 3rd, etc.)
function sheet_name = get_ordinal_suffix(iteration_number)
  if iteration_number == 1
    sheet_name = '1st iteration values';
  elseif iteration_number == 2
    sheet_name = '2nd iteration values';
  elseif iteration_number == 3
    sheet_name = '3rd iteration values';
  else
    sheet_name = [num2str(iteration_number), 'th iteration values'];
  end
end

% Function to generate the first 12 sets of parameters using log-normal distribution
function parameters = generate_parameters()
  % Define ranges for each parameter
  density_min = 7000;  density_max = 8100;
  youngs_modulus_min = 1.9e11;  youngs_modulus_max = 2.1e11;
  area_change_min = -20;  area_change_max = 0;  % Percentage change in area
  spring_stiffness_min = 50000;  spring_stiffness_max = 250000;

  % Generate 12 sets of parameters within the given ranges
  parameters = zeros(12, 4);
  for i = 1:12
    % Density (log-normal within specified range)
    parameters(i, 1) = generate_log_normal_range(density_min, density_max);

    % Young's Modulus (log-normal within specified range)
    parameters(i, 2) = generate_log_normal_range(youngs_modulus_min,
youngs_modulus_max);

    % Area Change (log-normal within specified range, as a negative percentage)
    parameters(i, 3) = -generate_log_normal_range(abs(area_change_max),
abs(area_change_min));

    % Longitudinal Stiffness (log-normal within specified range)
```

```
        parameters(i, 4) = generate_log_normal_range(spring_stiffness_min, spring_stiffness_max);
    end
end

% Function to generate the next set of parameters using GA-inspired approach
function parameters = generate_ga_parameters(top_parameters)
    % Define ranges for each parameter
    density_min = 7000;  density_max = 8100;
    youngs_modulus_min = 1.9e11;  youngs_modulus_max = 2.1e11;
    area_change_min = -20;  area_change_max = 0;
    spring_stiffness_min = 50000;  spring_stiffness_max = 250000;

    parameters = zeros(12, 4);

    % Generate parameters using crossover and mutation
    for i = 1:12
        % Select two parents randomly from the top parameters
        parents_idx = randperm(size(top_parameters, 1), 2);
        parent1 = top_parameters(parents_idx(1), :);
        parent2 = top_parameters(parents_idx(2), :);

        % Crossover: Take the average of the two parents
        child = (parent1 + parent2) / 2;

        % Mutation: Randomly perturb the child within the range (5% mutation)
        mutation_rate = 0.05;  % 5% mutation
        child(1) = min(max(child(1) * (1 + mutation_rate * (rand-0.5)), density_min),
density_max);
        child(2) = min(max(child(2) * (1 + mutation_rate * (rand-0.5)), youngs_modulus_min),
youngs_modulus_max);
        child(3) = min(max(child(3) * (1 + mutation_rate * (rand-0.5)), area_change_min),
area_change_max);
        child(4) = min(max(child(4) * (1 + mutation_rate * (rand-0.5)), spring_stiffness_min),
spring_stiffness_max);

        parameters(i, :) = child;
    end
end

% Function to generate a log-normal value within a specific range
function value = generate_log_normal_range(min_val, max_val)
    mean_val = (min_val + max_val) / 2;  % Calculate mean value
    sigma = 0.25;  % Standard deviation for log-normal distribution

    % Generate a log-normal random value within the range
    value = lognrnd(log(mean_val), sigma);
```

```
    % Ensure the generated value is within the specified range
    while value < min_val || value > max_val
        value = lognrnd(log(mean_val), sigma);
    end
end
```

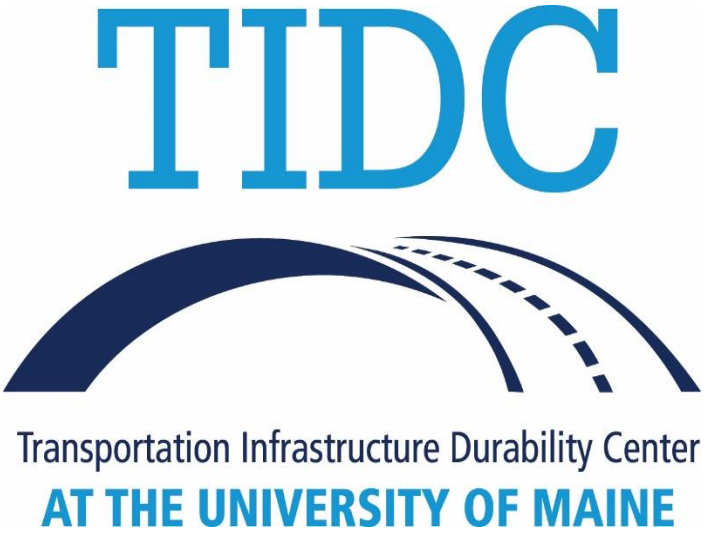

35 Flagstaff Road
Orono, Maine 04469
tidc@maine.edu
207.581.4376

www.tidc-utc.org